INTERNATIONAL JOURNAL FOR NUMERICAL METHODS IN ENGINEERING
Int. J. Numer. Meth. Engng 2005; **64**:1649–1677
Published online 11 August 2005 in Wiley InterScience (www.interscience.wiley.com). DOI: 10.1002/nme.1422

The element connectivity parameterization formulation for the topology design optimization of multiphysics systems

Gil Ho Yoon and Yoon Young Kim*, †

Multiscale Design Center and Integrated Design and Analysis of Structures Laboratory, School of Mechanical and Aerospace Engineering, Seoul National University, Seoul, Korea

SUMMARY

In spite of the success of the element-density-based topology optimization method in many problems including multiphysics design problems, some numerical difficulties, such as temperature undershooting, still remain. In this work, we develop an element connectivity parameterization (ECP) formulation for the topology optimization of multiphysics problems in order to avoid the numerical difficulties and yield improved results. In the proposed ECP formulation, finite elements discretizing a given design domain are not connected directly, but through sets of one-dimensional zero-length links simulating elastic springs, electric or thermal conductors. The discretizing finite elements remain solid during the whole analysis, and the optimal layout is determined by an optimal distribution of the inter-element connectivity degrees that are controlled by the stiffness values of the links. The detailed procedure for this new formulation for multiphysics problems is presented. Using one-dimensional heat transfer models, the problem of the element-density-based method is explained and the advantage of the ECP method is addressed. Copyright © 2005 John Wiley & Sons, Ltd.

KEY WORDS: topology optimization; multiphysics systems; undershooting; element connectivity

1. INTRODUCTION

Since the establishment of the topology optimization method [1], the method has been applied to various design problems including multiphysics system design problems [1–3]. Though several multiphysics systems are designed by the topology optimization method, some difficulties such as the incorrect prediction of some field distributions still remain. In this work, we develop an element connectivity parameterization (ECP) method for multiphysics problems in order to avoid the numerical difficulties and yield improved results. To pinpoint the cause of the difficulties and

*Correspondence to: Yoon Young Kim, Multiscale Design Center and Integrated Design and Analysis of Structures Laboratory, School of Mechanical and Aerospace Engineering, Seoul National University, Kwanak-Gu San 56-1, Seoul 151-742, Korea.
†E-mail: yykim@snu.ac.kr

Contract/grant sponsor: Korea Research Foundation; contract/grant number: KRF-2004-214-M01-2004-000-20114-0

Received 28 April 2004
Revised 24 May 2005
Accepted 24 May 2005

to explain the advantage of the ECP formulation, the current element-density-based topology optimization practice will be briefly reviewed.

The most popular design parameterization method for topology optimization is perhaps the so-called SIMP (solid isotropic material with penalization) method (see Reference [1]). In the SIMP method, real-valued continuously varying density variables are assigned to the finite elements discretizing a design domain and they are used as design variables. In structural problems, only the elastic property is assumed to be a penalized function of the density design variable. However, in multiphysics system design, more than one physical property should be modelled as the functions of the same density design variable. If all physical properties are not properly modelled, however, the solution of field problems for some range of the design variables can become physically incorrect.

As a specific multiphysics design problem, we will consider the topology optimization of an electro-thermal-compliant (ETC) actuator. If the SIMP approach is used for this problem, all of electric, thermal, and elastic properties are modelled as some functions of the same density variable, and if they are not properly modelled, some numerical problems can occur. When the SIMP modelling technique is used for the topology optimization involving heat transfer analysis, for instance, undershooting or overshooting problems occur. More discussions on this issue will be given below.

In formulating the topology optimization of multiphysics systems involving heat transfer analysis, two modelling strategies of the convection coefficient and the thermal conductivity have been suggested. In Reference [2], the thermal conductivity was assumed to vary as $\rho^{n_{\text{SIMP}}}$ ($n_{\text{SIMP}} \neq 0$) where ρ is the element density while the convection coefficient was assumed to be independent of ρ. On the other hand, the interpolation functions of the same form were used to model the thermal conductivity and the convection coefficient in Reference [3]. Regardless of the adopted models, the temperature distributions along the interfaces of the finite elements having certain density values turned out to be physically incorrect. For instance, the temperature at some nodes was lower than the room temperature. This problem, called undershooting, was indeed observed in Reference [2]. In this investigation, we will show theoretically why undershooting or overshooting cannot be avoided if the current element-density-based topology is used. We will also show that such numerical problems can be avoided when the proposed ECP method is employed.

Since it is difficult or impossible to avoid the above-mentioned numerical problem with the standard element-density method, we propose a different approach in which the degree of the element connectivity is used to represent a structural layout. This idea [4, 5] was originally developed to overcome the numerical instability problem appearing in the topology optimization of geometrically non-linear structures (see References [6–8] for geometrically non-linear design problems). The ECP method apparently was shown to effectively eliminate the instability problem resulting from unstable elements [4, 5]. In this investigation, we formulate the ECP method for multiphysics problems and show that the ECP method successfully avoids the problems such as undershooting.

The key idea of ECP may be illustrated with Figure 1. Figure 1 compares the design parameterizations by the conventional topology optimization formulation and the ECP formulation. Figure 1(b) illustrates the modelling of Figure 1(a) where all finite elements within the rectangular design domain are rigidly connected but the element densities have different values to represent the structure of Figure 1(a). Figure 1(c) illustrates the modelling of Figure 1(a) by the ECP approach where all finite elements have the original physical properties, but the element

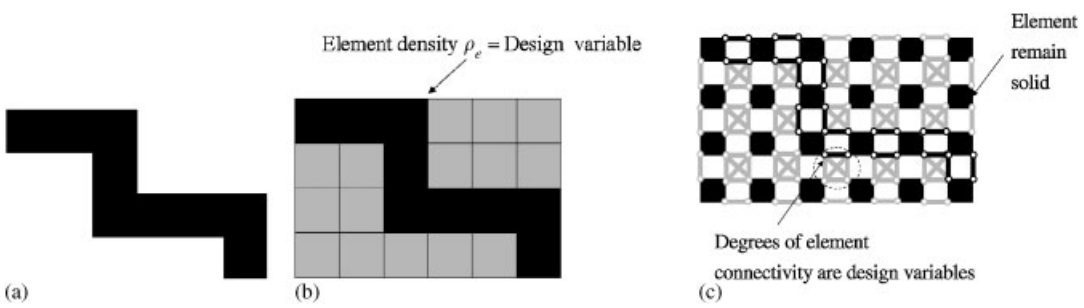

Figure 1. Comparison of the modelling techniques by the standard-element density-based method and the ECP method: (a) a given structure; (b) modelling by the element-density-based method; and (c) modelling by the ECP method.

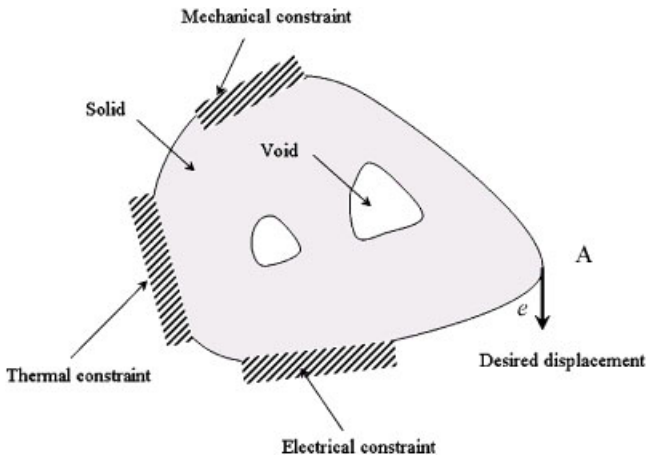

Figure 2. Topology optimization of an electro-thermal-compliant actuator.

connectivity degrees are allowed to vary to represent the structure of Figure 1(a). The element connectivity degrees are modelled by sets of one-dimensional zero-length links that connect the adjacent elements at a given location. In this work, the node will be called a connection because the finite elements discretizing a given design domain are not rigidly connected to each other at their common nodes. They are connected through the one-dimensional links, and the connectivity is controlled by the value of the link stiffness.

In pure structural problems, the links were interpreted as elastic springs [4, 5]. For the ETC-coupled design problems, we propose to interpret these links as zero-length electric conductors for electric problems and zero-length heat conductors for thermal problems. Then the link conductivities can be assumed as penalized functions of the link design variable.

The design of a geometrically non-linear ETC actuator shown in Figure 2 is a typical multiphysics design problem and the topology optimization of the actuator was done in

References [2, 3] by the element density approach. In this work, a special attention is paid to heat transfer problems to address the issue of undershooting or overshooting phenomena.

The actuator described in Figure 2 is supposed to generate force or displacement along the described direction under a given electric input. To calculate the performance of this actuator, it is required to analyse the following three field problems written in finite element matrix form (although non-linear structural analysis was performed for actual numerical calculation, only the linear equation will be presented without the loss of generality):

Electric problem (*symbol* E *used*)

$$\mathbf{K}_{\mathrm{E}}(\boldsymbol{\gamma})\mathbf{U}_{\mathrm{E}}(\boldsymbol{\gamma}) = \mathbf{F}_{\mathrm{E}}(\boldsymbol{\gamma}) \tag{1a}$$

Heat transfer problem (*symbol* T *used*)

$$\mathbf{K}_{\mathrm{T}}(\boldsymbol{\gamma})\mathbf{U}_{\mathrm{T}}(\boldsymbol{\gamma}) = \mathbf{F}_{\mathrm{T}}(\mathbf{U}_{\mathrm{E}}(\boldsymbol{\gamma}), \boldsymbol{\gamma}) \tag{1b}$$

Structural problem (*symbol* S *used*)

$$\mathbf{K}_{\mathrm{S}}(\boldsymbol{\gamma})\mathbf{U}_{\mathrm{S}}(\boldsymbol{\gamma}) = \mathbf{F}_{\mathrm{S}}(\mathbf{U}_{\mathrm{T}}(\boldsymbol{\gamma}), \boldsymbol{\gamma}) \tag{1c}$$

where $\boldsymbol{\gamma}$ is the array of design variables (In the element density approach, it denotes the element density), $\mathbf{U}_{\mathrm{E}}$, $\mathbf{U}_{\mathrm{T}}$, and $\mathbf{U}_{\mathrm{S}}$ the nodal values of the electric potential, the temperature, the displacement, respectively, and $\mathbf{K}_{(\circ)}$ and $\mathbf{F}_{(\circ)}$ ($\circ = \mathrm{E}, \mathrm{T}$ or S) the stiffness matrix and the force vector.

If the conventional element-density-based SIMP approach is used, the dependence of $\mathbf{K}_{(\circ)}$ ($\circ = \mathrm{E}, \mathrm{T}$ or S) on $\boldsymbol{\gamma}$ is written as

$$\mathbf{K}_{\mathrm{E}}(\boldsymbol{\gamma}) = \sum_{e=1}^{\mathrm{NE}} k_{\mathrm{E}}^{e}(\gamma_e), \quad \mathbf{K}_{\mathrm{T}}(\boldsymbol{\gamma}) = \sum_{e=1}^{\mathrm{NE}} (k_{\mathrm{T}}^{e}(\gamma_e) + k_{h}^{e}(\gamma_e)), \quad \mathbf{K}_{\mathrm{S}}(\boldsymbol{\gamma}) = \sum_{e=1}^{\mathrm{NE}} k_{\mathrm{S}}^{e}(\gamma_e) \tag{2a}$$

$$\mathbf{F}_{\mathrm{E}}(\boldsymbol{\gamma}) = 0, \quad \mathbf{F}_{\mathrm{T}}(\boldsymbol{\gamma}) = \sum_{e=1}^{\mathrm{NE}} f_{\mathrm{T}}^{e}(u_{\mathrm{E}}^{e}, \gamma_e), \quad \mathbf{F}_{\mathrm{S}}(\boldsymbol{\gamma}) = \sum_{e=1}^{\mathrm{NE}} f_{\mathrm{S}}^{e}(u_{\mathrm{T}}^{e}, \gamma_e) \tag{2b}$$

where NE denotes the number of finite elements and the element stiffness matrices $k_{(\circ)}^{e}$ and vectors $f_{(\circ)}^{e}$ ($\circ = \mathrm{E}, \mathrm{T}$ or S) are defined as

$$\begin{aligned} k_{\mathrm{E}}^{e}(\gamma_e) &= \int_{V_e} \sigma_{\mathrm{E}}(\gamma_e)\mathbf{B}^{\mathrm{T}}\mathbf{B}\,\mathrm{d}V, \quad k_{\mathrm{T}}^{e}(\gamma_e) = \int_{V_e} \sigma_{\mathrm{T}}(\gamma_e)\mathbf{B}^{\mathrm{T}}\mathbf{B}\,\mathrm{d}V \\ k_{h}^{e}(\gamma_e) &= \int_{\Gamma_{\mathrm{conv}}^{e}} h(\gamma_e)\mathbf{N}^{\mathrm{T}}\mathbf{N}\Gamma_{\mathrm{conv}}, \quad k_{\mathrm{S}}^{e}(\gamma_e) = \int_{V_e} \mathbf{B}^{\mathrm{T}}\mathbf{C}(\gamma_e)\mathbf{B}\,\mathrm{d}V \end{aligned} \tag{3a}$$

$$f_{\mathrm{T}}^{e}(\gamma_e) = \int_{\Gamma_{\mathrm{conv}}^{e}} h(\gamma_e)u_{\mathrm{T}}^{\infty}\mathbf{N}\,\mathrm{d}\Gamma_{\mathrm{conv}}, \quad f_{\mathrm{S}}^{e}(\gamma_e) = \int_{V_e} \mathbf{B}^{\mathrm{T}}\mathbf{C}(\gamma_e)\alpha(\gamma_e)(u_{\mathrm{T}}^{e} - u_{\mathrm{T}}^{\infty})\,\mathrm{d}V \tag{3b}$$

where $\mathbf{N}$ is the shape function matrix, $\mathbf{B}$ the strain (or gradient) interpolation matrix, $\Gamma_{\mathrm{conv}}^{e}$ the convection area of the eth element, V_e the domain of the eth element, $u_{(\circ)}^{e}$ ($\circ = \mathrm{E}$, T or S) the eth element's solution for each disciplinary, σ_{E} the electric conductivity, σ_{T} the thermal

conductivity, h the convection coefficient, u_{T}^{∞} the bulk or (room) temperature, $\mathbf{C}$ the elasticity tensor, and α the thermal expansion coefficient.

The specific topology optimization design problems considered in this work are as the followings:

1.1. Design of an electro-thermal-compliant actuator

Referring to Figure 2, the topology optimization of an ETC actuator can be written as

$$\text{maximize} \quad u_{\mathrm{S}} = \mathrm{L}^{\mathrm{T}}\mathbf{U}_{\mathrm{S}} \quad \text{(the displacement at A in the direction of } e\text{)} \tag{4a}$$

$$\text{subject to} \quad \sum_{e=1}^{\mathrm{NE}} \int_{V_e} \rho_e(\gamma_e) V_e \, \mathrm{d}V - M_0 \leqslant 0 \quad \text{(mass constraint)} \tag{4b}$$

$$(\hat{u}_{\mathrm{S}}/u_{\mathrm{S}})^2 \leqslant \varepsilon^* \quad \text{(cross-sensitivity constraint)} \tag{4c}$$

where $\hat{u}_{\mathrm{S}}$ denotes the displacement component at A in the perpendicular direction to e. The symbol L in the definition of u_{S} denotes a vector that has zero values except at the location corresponding to point A in Figure 2. The value $\varepsilon^* = 0.01$ was used for actual numerical calculation.

1.2. Design of a heat-dissipating structure

Since the numerical problem such as undershooting is related to heat transfer analysis during ETC actuator design optimization iterations, it is worth focusing on the topology optimization of heat transfer problems alone. The selected design problem is to find an optimal layout maximizing the thermal energy dissipation with a limit on the mass usage. Thus, the following optimization problem is set up:

$$\text{minimize} \quad Q = \int_{\Gamma_{\mathrm{source}}} q_{\mathrm{T}}^{\mathrm{T}} \mathbf{U}_{\mathrm{T}} \, \mathrm{d}\Gamma_{\mathrm{source}} \tag{5a}$$

$$\text{subject to} \quad \sum_{e=1}^{\mathrm{NE}} \int_{V_e} \rho_e(\gamma_e) V_e \, \mathrm{d}V - M_0 \leqslant 0 \quad \text{(mass constraint)} \tag{5b}$$

where q_{T} denotes heat flux into a domain of interest through its source boundary Γ_{source}. (The flux into the domain is assumed to be positive.)

2. ECP FORMULATION FOR MULTIPHYSICS SYSTEMS DESIGN OPTIMIZATION

To explain the key idea of the ECP formulation, let us begin with the modelling of the structure shown in Figure 1(a). As in the standard topology optimization formulation, the structure of Figure 1(a) is also enclosed inside a package (or design) domain in the ECP formulation. In the conventional element-based density method, weak materials are assigned to void regions, while strong materials are assigned to solid regions (i.e. the region occupied by a structure). In the ECP approach, however, the whole design domain is discretized by disconnected plane

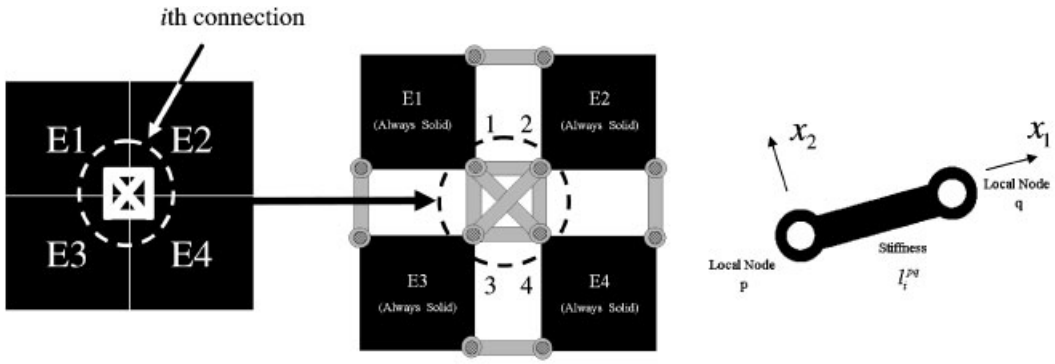

Figure 3. ECP modelling by six zero-length one-dimensional links at Connection i. (The local nodes are denoted by 1, 2, 3, and 4.)

finite elements having the original material property or the original stiffness, but the original structure is weaved by stiff zero-length links (see Figure 1(c)). On the other hand, the void region is weaved by very weak zero-length links. The links illustrated in Figure 1(c) have no length for actual numerical calculation, but they are plotted as if they have finite lengths for easier visualization of the result by the ECP modelling. In the ECP modelling, the magnitude of the link stiffness controls the connectivity degree between elements.

For more detailed description of the ECP modelling, consider the element connectivity at Connection i shown in Figure 3. There are four plane finite elements, E1–E4 around Connection i. In the ECP method, the four elements are not rigidly connected, but connected to each other by six one-dimensional links. If the stiffness of these links connecting local nodes 1 and 4 in Figure 3 is sufficiently large, the nodal displacements at nodes 1 and 4 can be treated as the same, i.e. nodes 1 and 4 can be assumed to be rigidly connected. If the stiffness of the link is very small, on the other hand, nodes 1 and 4 can be assumed to be disconnected. In the ECP modelling, therefore, the value of the link stiffness represents the element connectivity degree; by adjusting the link stiffness values, a given structural layout can be represented properly inside a package domain. The range of the link stiffness value will be given in Section 3.

In the ECP modelling, six links at Connection i can vary independently, so six independent design variables γ_i^{pq} $(p, q \in [1, 2, 3, 4],\ p \neq q\ )$ can be introduced at every connection. However, it is more convenient to use one unified design variable γ_i to control the element connectivity at Connection i (see References [4, 5] for the six variable modelling technique). This means that the stiffnesses of six links are always the same. If γ_i is used as the design variable controlling the link stiffness, one may penalize the link stiffness matrix $K^{\text{link}}_{i(pq)}$ connecting nodes p and q at Connection i as

$$K^{\text{link}}_{i(pq)} = l_0(\gamma_i)^{n_l} K^{\text{link}}_{(\circ),\text{nominal}} \quad \text{with } \gamma_{\text{Lower}} \leqslant \gamma_i \leqslant \gamma_{\text{Upper}} = 1 \quad (\circ = \text{E, T, and S}) \tag{6}$$

where l_0 is the upper bound of the link stiffness, and n_l is the penalty exponent used to push γ_i to its bounds as in the conventional SIMP approach. The value of l_0 should be large enough to impose the two nodal displacements to be virtually the same, but should be moderately large not to cause numerical instability. The symbol $K^{\text{link}}_{(\circ),\text{nominal}}$ denotes a dimensionless stiffness

matrix whose form varies with the involved principle. For example, consider two-dimensional structural problems for which every node has two degrees of freedom (the displacements in the x_1 and x_2 directions in Figure 3). In this case, l_0 implies the upper bound of the spring stiffness and $K^{\text{link}}_{\text{S,nominal}}$ becomes the following 4×4 symmetric matrix:

$$K^{\text{link}}_{\text{S,nominal}} = \begin{bmatrix} 1 & 0 & -1 & 0 \\ 0 & 1 & 0 & -1 \\ -1 & 0 & 1 & 0 \\ 0 & -1 & 0 & 1 \end{bmatrix} \tag{7}$$

For the electric or heat transfer problems, every node has only one degree of freedom representing the voltage potential or the temperature. In this case, l_0 implies the upper bound of the electrical conductivity or the thermal conductivity and $K^{\text{link}}_{(\circ),\text{nominal}}$ becomes a 2×2 matrix, $K^{\text{link}}_{\text{E,nominal}}$ or $K^{\text{link}}_{\text{T,nominal}}$

$$K^{\text{link}}_{\text{E,nominal}} = K^{\text{link}}_{\text{T,nominal}} = \begin{bmatrix} 1 & -1 \\ -1 & 1 \end{bmatrix} \tag{8}$$

Depending on the physics involved, the different interpretations of the zero-length links can be possible. For electric problems, the one-dimensional link can be interpreted as an electric conductor. If γ_i reaches γ_{Upper}, the link simulates an ideal electric one-dimensional conductor with very small or zero resistance. If γ_i reaches γ_{Lower}, the link simulates a non-conductor of electricity. For heat transfer problems, the link simulates an one-dimensional thermal conductor with the different conductivity. For other physical systems, similar interpretations can be possible.

In the ECP modelling, the plane finite elements used to discretized the design domain are connected through sets of zero-length one-dimensional links. Therefore, the global stiffness matrix $\mathbf{K}_{(\circ)}$ in the ECP approach ($\circ = \text{E, T, and S}$) consists of the two parts as

$$\mathbf{K}_{(\circ)}(\boldsymbol{\gamma}) = \bar{\mathbf{K}}_{(\circ)} + \mathbf{K}^{\text{link}}_{(\circ)}(\boldsymbol{\gamma}) \tag{9}$$

where $\bar{\mathbf{K}}_{(\circ)}$ is the stiffness matrix for the disconnected finite elements discretizing the design domain for each physical system. It is emphasized again that every element in $\bar{\mathbf{K}}_{(\circ)}$ is assumed to be disconnected to neighbouring elements. One can easily construct the associated stiffness matrix $\mathbf{K}_{(\circ)}(\boldsymbol{\gamma})$ if an in-house code is available. The ECP implementation is also quite straightforward with a commercial code as illustrated in Figure 4.

In the ECP approach, therefore, $\bar{\mathbf{K}}_{(\circ)}$ does not depend on the design variable $\boldsymbol{\gamma}$ and only $\mathbf{K}^{\text{link}}_{(\circ)}(\boldsymbol{\gamma})$ depends on the design variable. Perhaps, this is the key point of the ECP formulation. Because of this characteristics, the ECP modelling separates $\bar{\mathbf{K}}_{(\circ)}$ characterizing the system physics, either linear or non-linear, from $\mathbf{K}^{\text{link}}_{(\circ)}(\boldsymbol{\gamma})$ that depends explicitly on the design variable $\boldsymbol{\gamma}$. Therefore, the sensitivity analysis becomes extremely easy and the numerical problem such as the non-positive definiteness of the tangent stiffness matrix encountered in the conventional SIMP formulation of non-linear structural problems can be avoided.

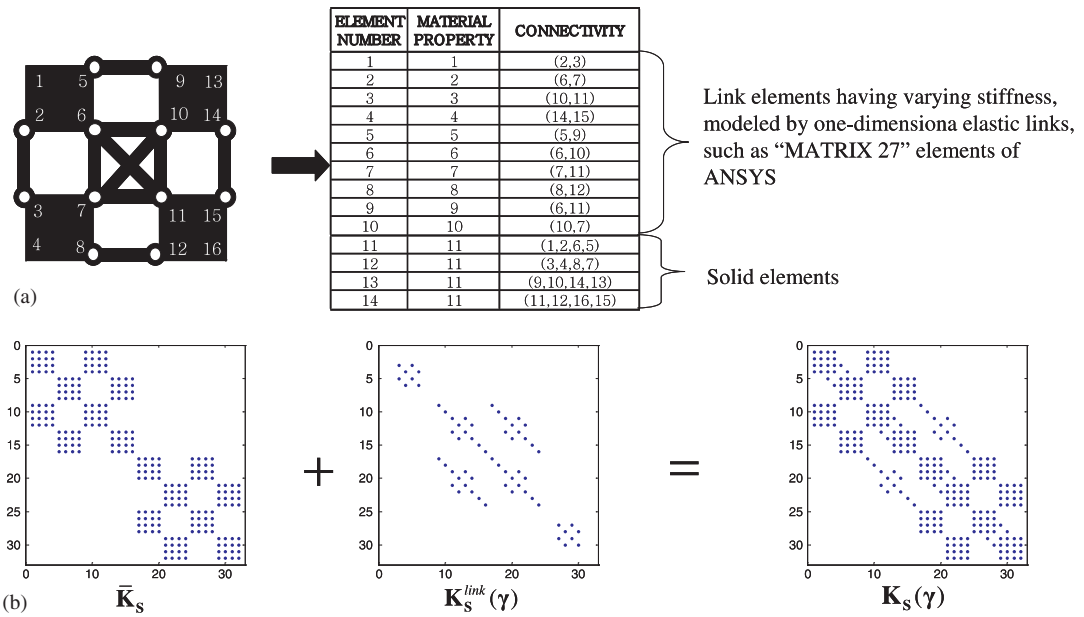

Figure 4. ECP modelling with ANSYS, a commercial finite element code: (a) modelling illustration; and (b) the structure of the assembled stiffness matrix for the ECP method.

Now, let us consider the sensitivity of the objective function u_S in (4) with respect to the design variable $\boldsymbol{\gamma}$ for the ECP method. Since the sensitivity analysis requires the solution of (3), it is convenient to introduce the adjoint variables $\boldsymbol{\lambda}_E$, $\boldsymbol{\lambda}_T$, and $\boldsymbol{\lambda}_S$ satisfying

$$(\mathrm{L}^{\mathrm{T}} + \boldsymbol{\lambda}_S^{\mathrm{T}}\mathbf{K}_S) = 0, \quad \left(\boldsymbol{\lambda}_T^{\mathrm{T}}\mathbf{K}_T - \boldsymbol{\lambda}_S^{\mathrm{T}}\frac{\partial \mathbf{F}_S}{\partial \mathbf{U}_T}\right) = 0, \quad \left(\boldsymbol{\lambda}_E^{\mathrm{T}}\mathbf{K}_E - \boldsymbol{\lambda}_T^{\mathrm{T}}\frac{\partial \mathbf{F}_T}{\partial \mathbf{U}_E}\right) = 0 \tag{10}$$

To facilitate the sensitivity analysis, we replace u_S in (4a) by the following expression:

$$u_S = \mathrm{L}^{\mathrm{T}}\mathbf{U}_S + \boldsymbol{\lambda}_E^{\mathrm{T}}(\mathbf{K}_E\mathbf{U}_E - \mathbf{F}_E) + \boldsymbol{\lambda}_T^{\mathrm{T}}(\mathbf{K}_T\mathbf{U}_T - \mathbf{F}_T) + \boldsymbol{\lambda}_S^{\mathrm{T}}(\mathbf{K}_S\mathbf{U}_S - \mathbf{F}_S) \tag{11}$$

Taking the derivative of u_S with respect to γ_i yields

$$\begin{aligned}\frac{\mathrm{d}u_S}{\mathrm{d}\gamma_i} = {} & \mathrm{L}^{\mathrm{T}}\frac{\mathrm{d}\mathbf{U}_S}{\mathrm{d}\gamma_i} + \boldsymbol{\lambda}_E^{\mathrm{T}}\left(\frac{\mathrm{d}\mathbf{K}_E}{\mathrm{d}\gamma_i}\mathbf{U}_E + \mathbf{K}_E\frac{\mathrm{d}\mathbf{U}_E}{\mathrm{d}\gamma_i} - \frac{\mathrm{d}\mathbf{F}_E}{\mathrm{d}\gamma_i}\right) \\ & + \boldsymbol{\lambda}_T^{\mathrm{T}}\left(\frac{\mathrm{d}\mathbf{K}_T}{\mathrm{d}\gamma_i}\mathbf{U}_T + \mathbf{K}_T\frac{\mathrm{d}\mathbf{U}_T}{\mathrm{d}\gamma_i} - \frac{\partial \mathbf{F}_T}{\partial \gamma_i} - \frac{\partial \mathbf{F}_T}{\partial \mathbf{U}_E}\frac{\mathrm{d}\mathbf{U}_E}{\mathrm{d}\gamma_i}\right) \\ & + \boldsymbol{\lambda}_S^{\mathrm{T}}\left(\frac{\mathrm{d}\mathbf{K}_S}{\mathrm{d}\gamma_i}\mathbf{U}_S + \mathbf{K}_S\frac{\mathrm{d}\mathbf{U}_S}{\mathrm{d}\gamma_i} - \frac{\partial \mathbf{F}_S}{\partial \gamma_i} - \frac{\partial \mathbf{F}_S}{\partial \mathbf{U}_T}\frac{\mathrm{d}\mathbf{U}_T}{\mathrm{d}\gamma_i}\right)\end{aligned} \tag{12}$$

Rearranging (12) gives

$$\frac{\mathrm{d}u_{\mathrm{S}}}{\mathrm{d}\gamma_i} = \left(\boldsymbol{\lambda}_{\mathrm{E}}^{\mathrm{T}}\mathbf{K}_{\mathrm{E}} - \boldsymbol{\lambda}_{\mathrm{T}}^{\mathrm{T}}\frac{\partial \mathbf{F}_{\mathrm{T}}}{\partial \mathbf{U}_{\mathrm{E}}}\right)\frac{\mathrm{d}\mathbf{U}_{\mathrm{E}}}{\mathrm{d}\gamma_i} + \left(\boldsymbol{\lambda}_{\mathrm{T}}^{\mathrm{T}}\mathbf{K}_{\mathrm{T}} - \boldsymbol{\lambda}_{\mathrm{S}}^{\mathrm{T}}\frac{\partial \mathbf{F}_{\mathrm{S}}}{\partial \mathbf{U}_{\mathrm{T}}}\right)\frac{\mathrm{d}\mathbf{U}_{\mathrm{T}}}{\mathrm{d}\gamma_i} + (\mathrm{L}^{\mathrm{T}} + \boldsymbol{\lambda}_{\mathrm{S}}^{\mathrm{T}}\mathbf{K}_{\mathrm{S}})\frac{\mathrm{d}\mathbf{U}_{\mathrm{S}}}{\mathrm{d}\gamma_i}$$
$$+ \boldsymbol{\lambda}_{\mathrm{E}}^{\mathrm{T}}\left(\frac{\mathrm{d}\mathbf{K}_{\mathrm{E}}}{\mathrm{d}\gamma_i}\mathbf{U}_{\mathrm{E}} - \frac{\mathrm{d}\mathbf{F}_{\mathrm{E}}}{\mathrm{d}\gamma_i}\right) + \boldsymbol{\lambda}_{\mathrm{T}}^{\mathrm{T}}\left(\frac{\mathrm{d}\mathbf{K}_{\mathrm{T}}}{\mathrm{d}\gamma_i}\mathbf{U}_{\mathrm{T}} - \frac{\partial \mathbf{F}_{\mathrm{T}}}{\partial \gamma_i}\right) + \boldsymbol{\lambda}_{\mathrm{S}}^{\mathrm{T}}\left(\frac{\mathrm{d}\mathbf{K}_{\mathrm{S}}}{\mathrm{d}\gamma_i}\mathbf{U}_{\mathrm{S}} - \frac{\partial \mathbf{F}_{\mathrm{S}}}{\partial \gamma_i}\right) \tag{13}$$

Substitute Equation (10) into Equation (13) yields the final result

$$\frac{\mathrm{d}u_{\mathrm{S}}}{\mathrm{d}\gamma_i} = \boldsymbol{\lambda}_{\mathrm{E}}^{\mathrm{T}}\left(\frac{\mathrm{d}\mathbf{K}_{\mathrm{E}}}{\mathrm{d}\gamma_i}\mathbf{U}_{\mathrm{E}} - \frac{\mathrm{d}\mathbf{F}_{\mathrm{E}}}{\mathrm{d}\gamma_i}\right) + \boldsymbol{\lambda}_{\mathrm{T}}^{\mathrm{T}}\left(\frac{\mathrm{d}\mathbf{K}_{\mathrm{T}}}{\mathrm{d}\gamma_i}\mathbf{U}_{\mathrm{T}} - \frac{\partial \mathbf{F}_{\mathrm{T}}}{\partial \gamma_i}\right) + \boldsymbol{\lambda}_{\mathrm{S}}^{\mathrm{T}}\left(\frac{\mathrm{d}\mathbf{K}_{\mathrm{S}}}{\mathrm{d}\gamma_i}\mathbf{U}_{\mathrm{S}} - \frac{\partial \mathbf{F}_{\mathrm{S}}}{\partial \gamma_i}\right) \tag{14}$$

To obtain $\mathrm{d}u_{\mathrm{S}}/\mathrm{d}\gamma_i$ in (14), the adjoint systems in (10) should be sequentially solved for the adjoint variables, $\boldsymbol{\lambda}_{\mathrm{S}}$, $\boldsymbol{\lambda}_{\mathrm{T}}$, and $\boldsymbol{\lambda}_{\mathrm{E}}$.

3. FEASIBLE SOLUTION FIELD BY ECP MODELLING

In the conventional element-density-based formulation, infeasible numerical solutions were obtained for certain density values [2]. In this section, we will investigate this issue theoretically using one-dimensional heat transfer problems. This investigation is followed by the numerical investigation of two-dimensional heat transfer problems. Through these investigations, we will emphasize that no infeasible solution is obtained when the ECP modelling technique is employed.

3.1. Theoretical analysis with one-dimensional model

3.1.1. Element-density-based modelling. Consider a one-dimensional heat transfer problem depicted in Figure 5(a). The analysis domain is discretized by two linear finite elements, Elements 1 and 2. The problem is to calculate the temperature distribution inside the one-dimensional body subject to a prescribed temperature $u_{\mathrm{T},1}^{1}$. The superscript e and the subscript i in $u_{\mathrm{T},i}^{e}$ denote the element number and the local node number, respectively. The bulk or room temperature is denoted by u_{T}^{∞}. Using the standard finite element formulation (see References [9, 10] for details or Appendix A), the following element-level matrix equation can be obtained:

$$[k_{\mathrm{T}}^{e} + k_{h}^{e}]\begin{Bmatrix} u_{\mathrm{T},1}^{e} \\ u_{\mathrm{T},2}^{e} \end{Bmatrix} = \begin{Bmatrix} f_{\mathrm{T},1}^{e} + \hat{f}_{\mathrm{T},1}^{e} \\ f_{\mathrm{T},2}^{e} + \hat{f}_{\mathrm{T},2}^{e} \end{Bmatrix} \tag{15}$$

where

$$k_{\mathrm{T}}^{e} = \frac{\mathrm{A}_e\sigma_e}{\mathrm{L}_e}\begin{pmatrix} 1 & -1 \\ -1 & 1 \end{pmatrix} \tag{16a}$$

$$k_{h}^{e} = \frac{h_e\mathrm{P}_e\mathrm{L}_e}{6}\begin{pmatrix} 2 & 1 \\ 1 & 2 \end{pmatrix} \tag{16b}$$

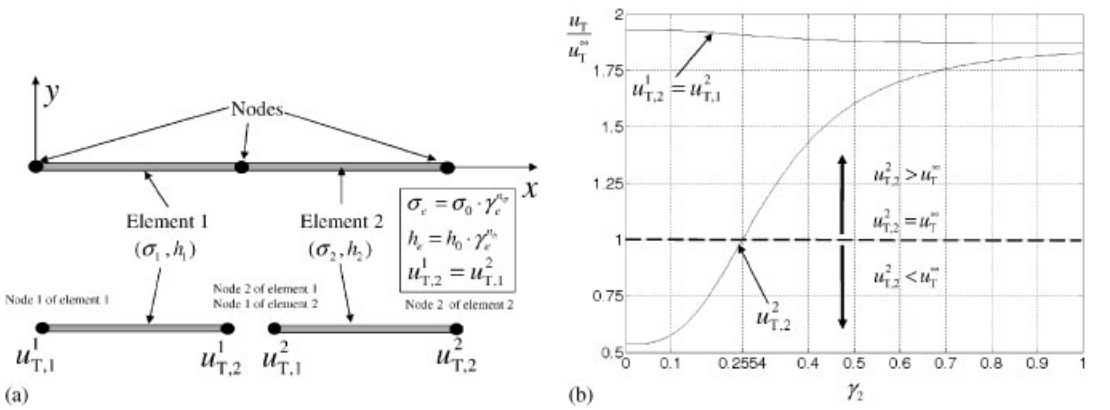

Figure 5. Theoretical analysis of the temperature variations in one-dimensional heat transfer problems for varying density values. ($u^1_{T,1} = 600$, $u^\infty_T = 300$): (a) two finite-element model; and (b) the variation of $u^1_{T,2}$ and $u^2_{T,2}$ as the function of γ_2 (γ_1 fixed as unity).

$$f^e_{T,i} = \frac{h_e u^\infty_T P_e L_e}{2} \quad (i = 1, 2) \tag{16c}$$

The symbol $\hat{f}^e_{T,i}$ is the concentrated heat flow input at node i of element e. In (16), A_e, L_e, and P_e denote the cross-sectional area, the length, and the perimeter of the eth element.

Let us examine the solution behaviour when the thermal conductivity σ_e and the heat convection coefficient h_e vary as the functions of the element density variable γ_e ($0 \leqslant \gamma_e \leqslant 1$). This situation simulates the design parameterization of the standard element-density-based approach. If the SIMP modelling is employed, $\sigma_e(\gamma_e)$ and $h_e(\gamma_e)$ can be written as

$$\sigma_e = \sigma_0(\gamma_e)^{n_\sigma}, \quad h_e = h_0(\gamma_e)^{n_h} \quad (e = 1, 2) \tag{17}$$

where the subscript 0 stands for the nominal value, and (n_σ, n_h) are the orders of the polynomials. To simplify numerical calculations, the following numerical values (units are ignored) will be used without the loss of generality:

$$\sigma_0 = 10, \quad h_0 = 1, \quad A_e = L_e = P_e = 1, \quad u^\infty_T = 300, \quad u^1_{T,1} = 600 \tag{18}$$

Using the conditions $u^2_{T,1} = u^1_{T,2}$ and $\hat{f}^1_{T,1} = 0$, $\hat{f}^1_{T,2} + \hat{f}^2_{T,1} = 0$, $\hat{f}^2_{T,2} = 0$ (i.e. no concentrated heat flow input), the following system equation can be formed:

$$\begin{pmatrix} \sigma_1 + \frac{h_1}{3} & -\sigma_1 + \frac{h_1}{6} & 0 \\ -\sigma_1 + \frac{h_1}{6} & \sigma_1 + \frac{h_1}{3} + \sigma_2 + \frac{h_2}{3} & -\sigma_2 + \frac{h_2}{6} \\ 0 & -\sigma_2 + \frac{h_2}{6} & \sigma_2 + \frac{h_2}{3} \end{pmatrix} \begin{pmatrix} u^1_{T,1} \\ u^1_{T,2} (= u^2_{T,1}) \\ u^2_{T,2} \end{pmatrix} = \begin{pmatrix} \frac{h_1 u^\infty_T}{2} + 0 \\ \frac{h_1 u^\infty_T}{2} + \frac{h_2 u^\infty_T}{2} + 0 \\ \frac{h_2 u^\infty_T}{2} + 0 \end{pmatrix} \tag{19}$$

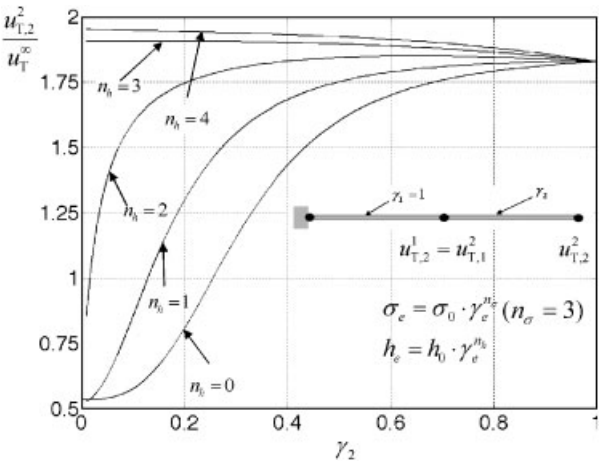

Figure 6. The solution behaviour of $u^2_{T,2}$ for varying values of n_h when $h_2 = h_0\gamma_2^{n_h}$ (theoretically, $u^2_{T,2}$ should approach u^∞_T as γ_2 goes to zero).

To examine the solution behaviour as γ_e varies, γ_1 is set as unity, (equivalently, Element 1 has the nominal property) and only γ_2 will be varied. Using the data in (18), the nodal temperatures are calculated as

$$u^1_{T,2}(\gamma_2) = u^2_{T,1}(\gamma_2) = \frac{300[3(\gamma_2^{n_h})^2 + 7260\gamma_2^{n_\sigma} + \gamma_2^{n_h}(242 + 360\gamma_2^{n_\sigma})]}{3(\gamma_2^{n_h})^2 + 3720\gamma_2^{n_\sigma} + 4\gamma_2^{n_h}(31 + 90\gamma_2^{n_\sigma})} \tag{20a}$$

$$u^2_{T,2}(\gamma_2) = \frac{300[3(\gamma_2^{n_h})^2 + 7260\gamma_2^{n_\sigma} + \gamma_2^{n_h}(65 + 360\gamma_2^{n_\sigma})]}{3(\gamma_2^{n_h})^2 + 3720\gamma_2^{n_\sigma} + 4\gamma_2^{n_h}(31 + 90\gamma_2^{n_\sigma})} \tag{20b}$$

Let us choose $n_\sigma = 3$ and $n_h = 0$ as in the topology optimization formulation [2] (i.e. h_2 is independent of γ_2) and check the solution behaviour. Figure 5(b) shows the behaviour of $u^1_{T,2}(\gamma_2) = u^2_{T,1}(\gamma_2)$ and $u^2_{T,2}(\gamma_2)$ as the function of γ_2. When γ_2 reaches zero, no material in Element 2 exists. In this limit, $u^2_{T,2}(\gamma_2)$ must approach u^∞_T, but the plot in Figure 5(b) shows that $u^2_{T,2}(\gamma_2)$ becomes even lower than u^∞_T as long as $\gamma_2 < 0.2554$. Obviously, this is physically unacceptable or infeasible. This problem was reported as the undershooting problem in Reference [2], which may not be avoided as long as σ_e and h_e are interpolated as the function of the element density variable. If this problem occurs in the ETC actuator design problem, the structural region having undershot temperature will shrink, not expand. So the quality of the optimized result may be affected.

One may now wonder what will happen if different values of n_h are used instead of $n_h = 0$. ($n_\sigma = 3$ is set without the loss of generality) To investigate the effect of n_h on the solution, we varied n_h from 0 to 4 and plotted $u^2_{T,2}(\gamma_2)$ in Figure 6. Before examining Figure 6, it is noted that the exact solution of $u^2_{T,2}$ must be equal to u^∞_T as γ_2 approaches zero. When $n_h < n_\sigma$, however, $u^2_{T,2}$ drops below the room temperature u^∞_T as γ_2 approaches 0. If $n_h \geqslant n_\sigma$, on the other hand, $u^2_{T,2}$ becomes higher than u^∞_T as γ_2 approaches 0. That is, the temperature at node

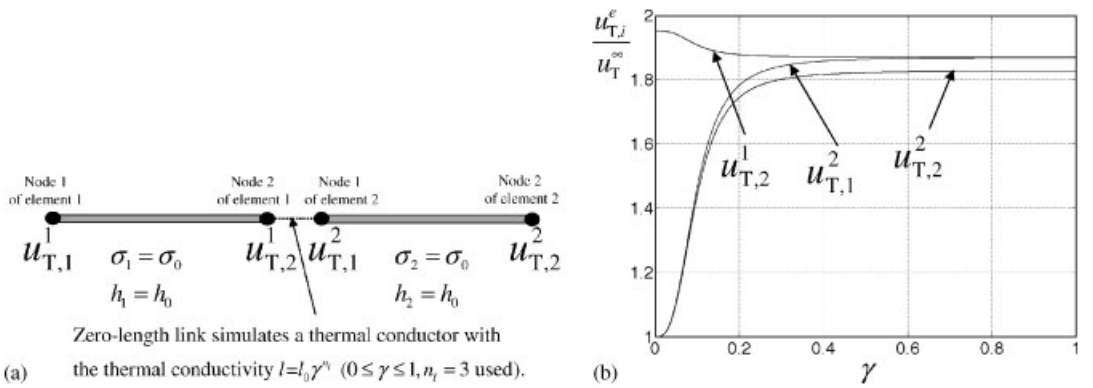

Figure 7. Theoretical analysis for one-dimensional heat transfer problems by the ECP modelling: (a) one-dimensional model by ECP; and (b) the variation of $u^e_{T,i}$ as the function of γ.

2 of Element 2 is overshot. Yin and Ananthasuresh [3] used some interpolation functions of σ_e and h_e different from $\sigma_0\gamma_e^{n_\sigma}$ and $h_0\gamma_e^{n_h}$, but their functions can be regarded as (17) with the same values of n_σ and n_h. From this one-dimensional analysis, it is clearly shown that physically infeasible or inaccurate solutions cannot be avoided if σ_e and h_e are treated as the functions of the element density variables.

3.1.2. ECP modelling. Let us now investigate the solution behaviour when the ECP modelling technique is employed. Figure 7(a) shows the ECP-based model that is equivalent to the element-density-based model in Figure 5(a). The matrix equations for Elements 1 and 2 are the same as (15), but σ_e and h_e $(e = 1, 2)$ have the nominal values σ_0 and h_0 in this ECP modelling. The matrix equation for the zero-length link is

$$l \begin{bmatrix} 1 & -1 \\ -1 & 1 \end{bmatrix} \begin{Bmatrix} u^1_{T,2} \\ u^2_{T,1} \end{Bmatrix} = \begin{Bmatrix} f^1_{T,2} \\ f^2_{T,1} \end{Bmatrix} \tag{21}$$

where l is the thermal conductivity varying from zero to l_0 as

$$l = l_0\gamma^{n_l} \quad (\gamma_{\text{lower}} \leqslant \gamma \leqslant \gamma_{\text{upper}}) \tag{22}$$

In the ECP modelling, the element connectivity is controlled by the value of l. If l becomes l_0 or zero, Elements 1 and 2 are treated as being rigidly connected or disconnected. To reach the states of rigid connection or no connection correctly, the value of l_0 and γ_{lower} should be selected appropriately.

Our guideline for l_0 and γ_{lower} is

$$\begin{gathered} l_0 \approx 1000k \\ \gamma_{\text{lower}} \approx 0.01 \quad \text{if } n_l = 3 \sim 5 \end{gathered} \tag{23}$$

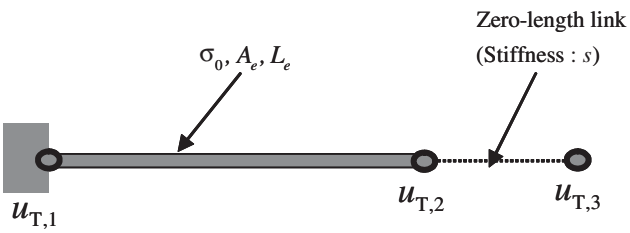

Figure 8. A simple one-dimensional example.

where k implies the diagonal term of the element stiffness matrix in Equation (15). To support the validity of the suggested values of l_0 and γ_{lower}, a simple one-dimensional one-element heat conduction model in Figure 8 is considered. (The nodes in Figure 8 are globally numbered.)

To investigate the solution behaviour for varying values of γ with the suggested values of l_0 and γ_{lower}, the stiffness matrix relating $(u_{\text{T},1}, u_{\text{T},3})$ and (f_1, f_3) is obtained:

$$\frac{sk}{s+k}\begin{bmatrix} 1 & -1 \\ -1 & 1 \end{bmatrix}\begin{bmatrix} u_{\text{T},1} \\ u_{\text{T},3} \end{bmatrix} = \begin{bmatrix} f_1 \\ f_3 \end{bmatrix} \tag{24}$$

where s is the link stiffness. In Equation (24), f_i and $u_{\text{T},i}$ are the nodal heat input and temperature at node i. If heat conduction is considered alone, k is simply $\sigma_e \mathrm{A}_e/\mathrm{L}_e$ (see Equation (16a)). Note that the heat is assumed to be introduced through node 3, not node 2. If the link stiffness is penalized as $s = l_0\gamma^{n_l}$ and the suggested values of l_0 and γ_{lower} in (23) are used, the following results are obtained (with $n_l = 5$)

$$\text{if} \quad \gamma = \gamma_{\text{lower}} = 0.01, \quad s = 10^{-7}k \quad \text{and} \quad \frac{s}{s+k} = 1.0 \times 10^{-7}\left(\left.\frac{s}{s+k}\right|_{\text{exact}} = 0.000\right)$$

$$\text{if} \quad \gamma = \gamma_{\text{upper}} = 1, \quad s = 10^{3}k \quad \text{and} \quad \frac{s}{s+k} = 0.999\left(\left.\frac{s}{s+k}\right|_{\text{exact}} = 1.000\right)$$

As shown above, the stiffness of the modified system by the link approaches the exact value within the error of 0.01% in the limits of γ_{lower} and γ_{upper}.

Back to the model in Figure 7(a), the following system matrix of the whole configuration is considered:

$$\begin{pmatrix} \sigma_0 + \frac{h_0}{3} & -\sigma_0 + \frac{h_0}{6} & 0 & 0 \\ -\sigma_0 + \frac{h_0}{6} & \sigma_0 + \frac{h_0}{3} + l & -l & 0 \\ 0 & -l & \sigma_0 + \frac{h_0}{3} + l & -\sigma_0 + \frac{h_0}{6} \\ 0 & 0 & -\sigma_0 + \frac{h_0}{6} & \sigma_0 + \frac{h_0}{3} \end{pmatrix} \begin{pmatrix} u^1_{\text{T},1} \\ u^1_{\text{T},2} \\ u^2_{\text{T},1} \\ u^2_{\text{T},2} \end{pmatrix} = \begin{pmatrix} \frac{h_n u^{\infty}_{\text{T}}}{2} \\ \frac{h_n u^{\infty}_{\text{T}}}{2} \\ \frac{h_n u^{\infty}_{\text{T}}}{2} \\ \frac{h_n u^{\infty}_{\text{T}}}{2} \end{pmatrix} \tag{25}$$

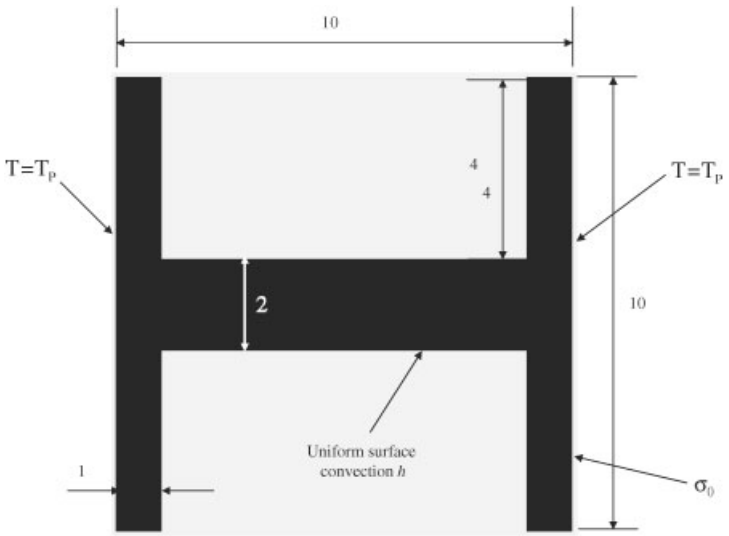

Figure 9. A two-dimensional heat transfer problem defined in an H-shaped structure. ($\sigma_0 = 10,\ h_0 = 1,\ u_{\mathrm{T}}^{\infty} = 300,\ \mathrm{T_P} = 600$).

Using $l_0 = 1000$ and the numerical data given in (18), one obtains

$$\begin{pmatrix} u_{\mathrm{T},2}^{1} \\ u_{\mathrm{T},1}^{2} \\ u_{\mathrm{T},2}^{2} \end{pmatrix} = \frac{1}{3751 + 4207000 \times \gamma^{n_l}} \begin{pmatrix} 18150(121 + 130000 \times \gamma^{n_l}) \\ 36300(31 + 65000 \times \gamma^{n_l}) \\ 9300(121 + 248000 \times \gamma^{n_l}) \end{pmatrix} \tag{26}$$

Figure 7(b) shows the nodal temperature variation as the function of γ. When the ECP modelling is employed, the temperature always remains feasible for all values of γ. In particular, $u_{\mathrm{T},1}^{2}$ and $u_{\mathrm{T},2}^{2}$ behave correctly as γ approaches zero. Therefore, one can see that the ECP modelling technique can simulate all material distribution states from solid to void by varying γ of the zero-length link while the temperature distribution remains feasible for all values of γ.

3.2. Numerical analysis with two-dimensional model

The theoretical analysis carried out with a one-dimensional model may be extended to the case of two-dimensional problems. For two-dimensional cases, however, we investigated the solution behaviour numerically. Figure 9 shows a two-dimensional problem defined in an H-shaped structure. Figure 10 shows three modelling techniques. The mesh refinements for two models in Figures 10(b) and (c) are identical. The embedded model in Figure 10(b) results from the standard element-density method ($n_\sigma = 3,\ n_h = 0$ as in Reference [2]) and the embedded model in Figure 10(c) results from the proposed ECP method. Figure 11 compares the temperature distributions along the centreline C1–C2 obtained by the element-density-based modelling technique and by the ECP modelling technique. The direct model refers to the model

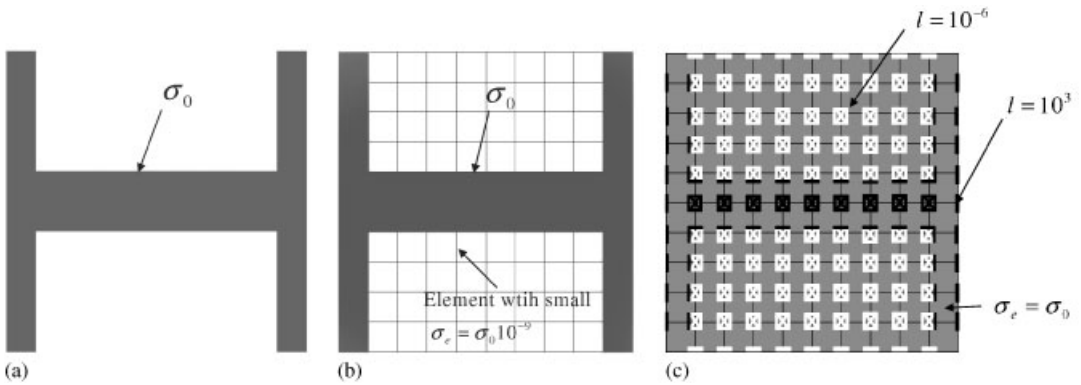

Figure 10. Three modelling techniques for the analysis of the H-shaped structure shown in Figure 9: (a) direct modelling; (b) embedded model in a package domain by the element-density method; and (c) embedded model in a package domain by ECP.

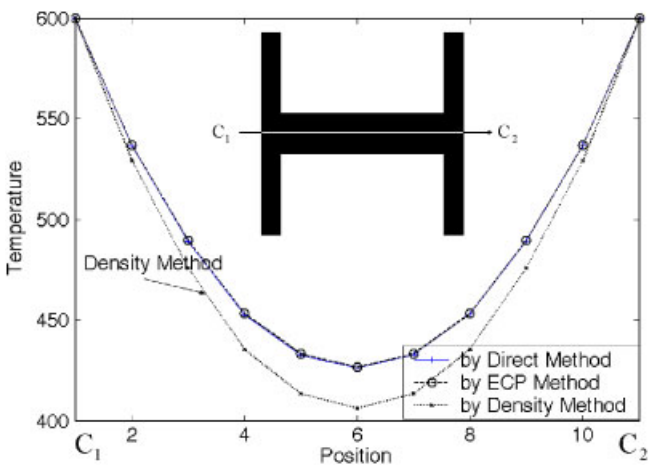

Figure 11. The centreline temperature distribution calculated by different modelling methods.

consisting of the finite element discretizing the H-shaped structure alone, not including the rest of the package domain. Figure 11 shows that the temperature (T_{EDM}) by the element-density method is quite off from the temperature (T_{DMM}) by the direct modelling method. On the other hand, the temperature (T_{ECP}) by the proposed ECP method is almost the same as T_{DMM}. To see the reason for the inaccuracy in T_{EDM}, the temperature distribution inside the whole package domain is examined in Figure 12. Unlike T_{ECP}, the T_{EDM} distribution by the element-density method has lower temperature than the bulk temperature at some nodes near solid–void interface boundaries. This is exactly the same undershooting problem that was observed in the one-dimensional problem. This numerical example shows that the solution by the ECP method is feasible and very accurate.

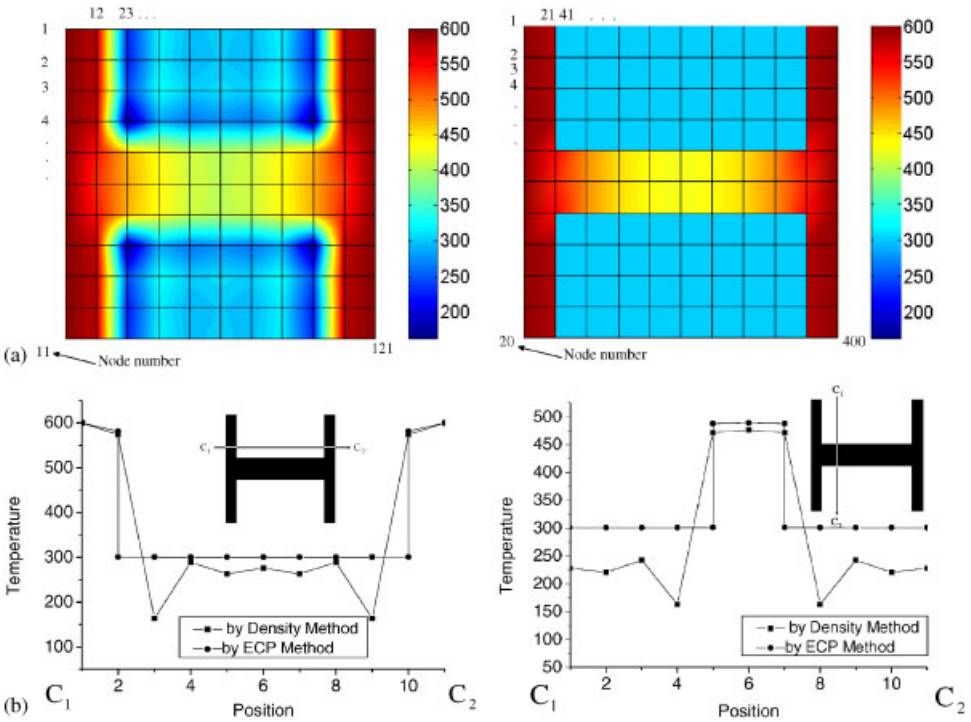

Figure 12. The temperature distribution inside the package domain: (a) temperature on the plane; and (b) the temperature at the sections.

3.3. Remarks

If more accurate heat transfer analysis is needed, one may consider the side convection [3]. In the standard element-density-based method, it is difficult to incorporate the side convection for topology optimization. However, it is quite easy to take into account the side convection in the ECP method. This issue will be explained below.

Consider a plane element shown in Figure 13(a), which is surrounded by four sets of links. Here, the links simulate heat conductors. Since the element connectivity between plane finite elements is imposed only at the node in the ECP method, side convection can be easily incorporated. For instance, if Side 4 of the plane element is disconnected from its neighbouring element ($\gamma_1 = 0$ and $\gamma_4 = 0$) in the ECP method, side convection should take place on this side as in Figure 13(b). On the contrary, when Side 4 is connected to its neighbouring element ($\gamma_1 = 1$ and $\gamma_4 = 1$), no side convection should occur through this side, but heat conduction should occur when ECP is used. The physical behaviour mentioned above can be easily modelled by interpolating the side convection coefficient h_q^{side} $(q = 1, 2, 3, 4)$ as

$$h_1^{\text{side}} = h_0 \times (1 - (\gamma_1\gamma_2)^{n_h^{\text{side}}}), \quad h_2^{\text{side}} = h_0 \times (1 - (\gamma_2\gamma_3)^{n_h^{\text{side}}})$$
$$h_3^{\text{side}} = h_0 \times (1 - (\gamma_3\gamma_4)^{n_h^{\text{side}}}), \quad h_4^{\text{side}} = h_0 \times (1 - (\gamma_1\gamma_4)^{n_h^{\text{side}}}) \tag{27}$$

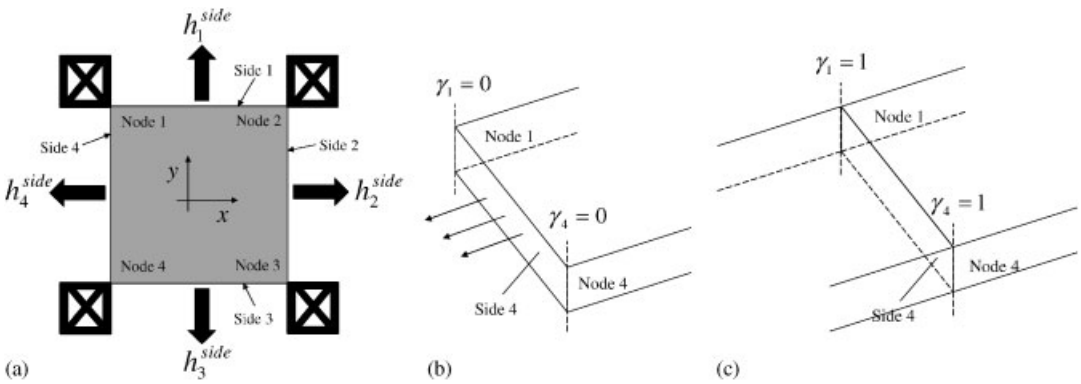

Figure 13. Modelling issue of the side convection (the surface convection in z considered for analysis, but no depicted here): (a) two-dimensional element surrounded by four sets of one-dimensional zero-length links; (b) side convection at Side 4 when $\gamma_1 = \gamma_4 = 0$; and (c) conduction through Side 4 when $\gamma_1 = \gamma_4 = 1$.

when n_h^{side} is the penalty exponent. (We will use $n_h^{\text{side}} = n^l$ for all numerical calculation without loss of generality.) The side convection model in (27) will be used whenever the side convection needs to be considered.

The modelling issue related to heat transfer analysis was mainly discussed. It was shown that when more than one physical property is interpolated by the element density variable, infeasible solutions such as the undershoot temperature could occur. If fully coupled multi-physics design optimization problems are solved by the element-density-based approach, the situation will be even severe. Because of the difficulty in modelling, no unified form of the interpolation function for the thermal expansion coefficient α was available within the element-density-based approach. The expansion coefficient was treated as an independent function of the element density in Reference [2] and as a dependent function of the element density in Reference [3]. However, no such difficulty arises in the ECP approach. The length of the link is zero, so the thermal expansion only takes place in the discretizing finite elements.

A few remarks on non-linear analysis will be made. The topology optimization of the ETC actuator may require geometrically non-linear analysis for large deformation. When the element-density-based formulation is employed, the tangent stiffness of the elements having low densities can become singular. As a result, the elements become unstable, so convergence problems may occur. However, it is shown in References [4, 5] that the problem of unstable elements does not occur when the ECP method is employed. Even if the actual structural analysis requires non-linear analysis, the links connecting the elements discretizing the design domain can be modelled simply as linear elastic links. In this work, the non-linear elastic analysis was carried out by employing the ECP formulation given in References [4, 5], so the detail account on the non-linear analysis will not be given here.

The main disadvantage of the ECP formulation is the increase in the size of the system matrix. Since all finite elements are connected not rigidly but by length-zero links, the total degrees of freedom for the system matrix increase. For two-dimensional problems, the size of the system matrix for the ECP approach is almost four times as large as the size for the

element-density method. Therefore, more computation time will be required. However, the increase in the system matrix size may not be a serious problem since the computation time for the topology optimization of geometrically non-linear structures by the ECP method took considerable less computation time [4, 5] because no unstable element appears in the ECP formulation.

4. NUMERICAL EXAMPLES

The effectiveness of the ECP method will be checked by the topology optimization of heat-dissipating structures and geometrically non-linear ETC actuators. For all optimization problems, the method of moving asymptotes [11, 12] was employed. For all numerical analyses, standard four-node bilinear finite elements were used.

4.1. Structural layout identification

To identify the structural layout from a given or optimized distribution of $\boldsymbol{\gamma}$, two schemes may be used. The first scheme is called the skeleton-imaging scheme which is illustrated in Figure 14(b). In this scheme, the horizontal and vertical lengths of the links are assumed to be proportional to the sizes of their adjacent analysis plane finite elements. In this scheme, the original plane elements are not plotted. The second scheme is called as the raster-imaging scheme illustrated in Figure 14(c). The optimized values of the design variables γ_i are used to render the finite elements. If an eth element is surrounded by four links $(\gamma_1, \gamma_2, \gamma_3, \gamma_4)$, its darkness will be proportional to its average, $(\gamma_1+\gamma_2+\gamma_3+\gamma_4)/4$ but the element densities are not the design variables in the ECP formulation.

To explain the connection between the rastered layout obtained by the averaging and the original layout connected by the links, let us consider the structural responses of a skeleton image and a raster image in Figure 15. If the applied load F is of the same magnitude, the displacements obtained with the skeleton layout (modelled by ECP) and the raster layout (post-processed by the averaging) are those given in Table I.

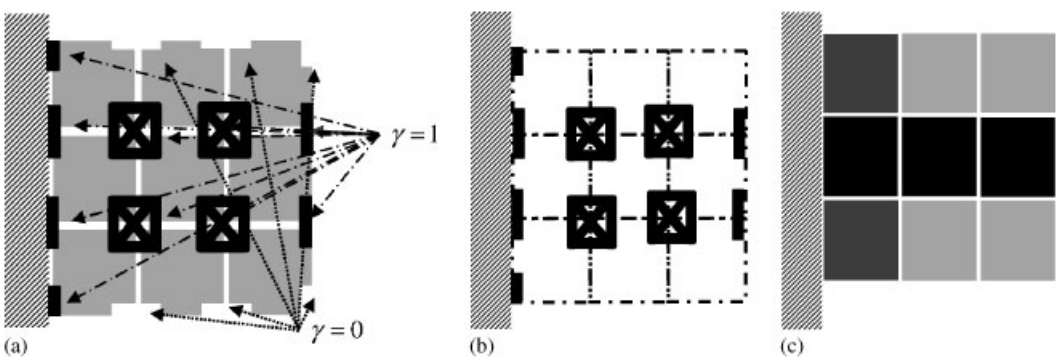

Figure 14. Representation of a structural layout: (a) the distribution of the link design variables; (b) skeleton-imaging method; and (c) raster-imaging method.

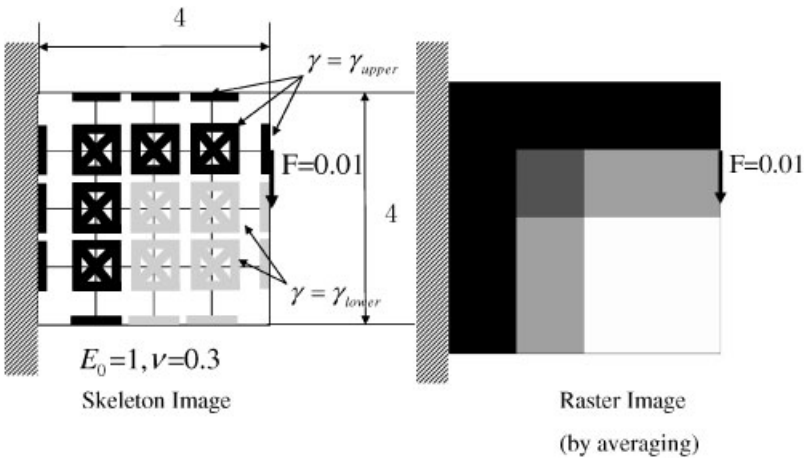

Figure 15. A simple test to compare the structural behaviour of the skeleton layout and the post-processed raster layout.

Table I. Comparison of the displacement by ECP and the displacement by a post-processed raster image.

Displacement with the raster layout	0.446 If $n_{\mathrm{SIMP}} = 3$	0.448 If $n_{\mathrm{SIMP}} = 3.61564$	0.4918 If $n_{\mathrm{SIMP}} = 4$
Displacement with the skeleton layout (present ECP)		0.448	

For structural analysis, we used E_0 (Young's modulus) $= 1.0$, v (Poisson's ratio) $= 0.3$. The stiffness of the intermediate-density element for results in Table I was penalized by SIMP as

$$\underbrace{E(\rho_e)}_{\text{from the raster image}} = E_0 \underbrace{\rho_e^{n_{\mathrm{SIMP}}}}_{\text{from the raster image}} \tag{28}$$

As illustrated in Table I, the displacements with the skeleton layout and the post-processed raster layout can be identical if the intermediate-density element stiffness is properly interpolated. From this comparison, one can see that if necessary, the skeleton layout can be interpreted as an equivalent element-density-based layout. It is remarked that the rastered elements may have intermediate-density values even if the link design variables have reached lower or upper bounds because of the nodal averaging. Similar problems were also observed when nodal density approaches were employed in the conventional element density formulation. If the number of the design variables is large, however, the usual post-processing technique can yield clear white-and-black images that are sufficient in identifying the optimal layout.

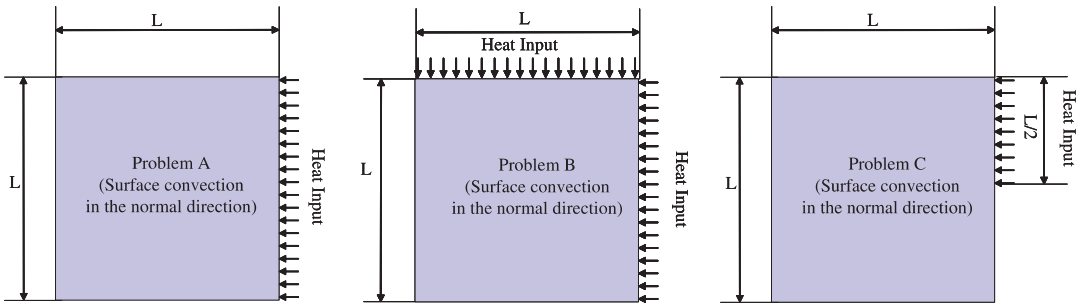

Figure 16. Problem definition for the design of heat-dissipating structures ($L = 40$, thermal conductivity $= 1$, surface convection coefficient $= 0.002$, uniform heat input $= 0.5$ at nodes, bulk temperature $u_T^{\infty} = 0$, and the mass constraint $= 40\%$ of design domain, and 40×40 finite element discretization. Both nodes and elements are numbered downward from the left to the right).

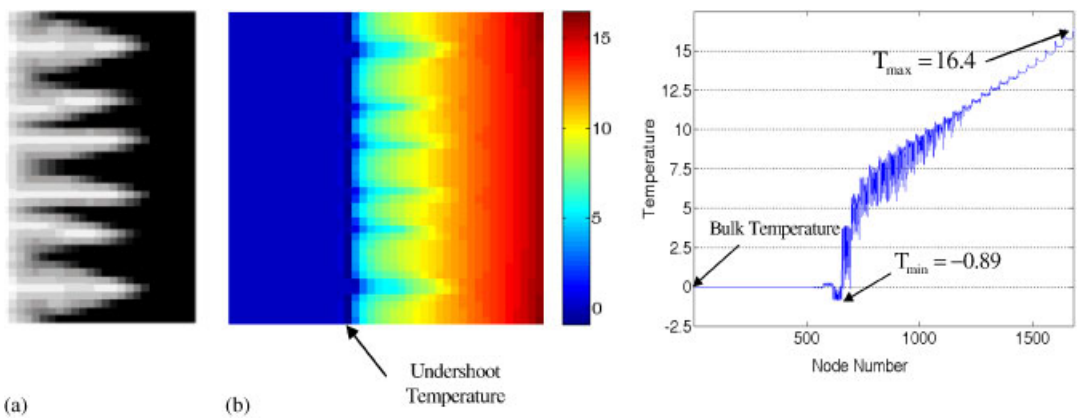

Figure 17. The optimized result for Problem A by the SIMP approach ($n_\sigma = 3$, $n_h = 0$): (a) density distribution; and (b) temperature plot.

Case 1: Design of heat-dissipation structures.

The objective is to find the most effective heat-dissipating structure subjected to a prescribed heat input. Three design problems were considered as depicted in Figure 16, which are designated as Problem A, Problem B, and Problem C depending on the heat input condition. Figure 17 shows the results by the density-based SIMP approach with $n_\sigma = 3$ and $n_h = 0$ for Problem A. As in the one-dimensional problem, the temperature near solid–void interface was undershot. It is interesting to see the effect on n_h (with n_σ fixed) on the optimized results. Figure 18 compares the results by $n_h = 1, 2, 3$ and 4. If $n_h \geqslant n_\sigma$, the temperature undershooting problems disappeared, but the resulting layouts were not satisfactory due to the temperature overshooting as predicted by Figure 6. Adjusting the parameters of the optimizer and the problem definition may yield better results, but it was not pursued as the main objective of varying n_h was to show the effect of n_h/n_σ on the behaviour of the temperature distribution.

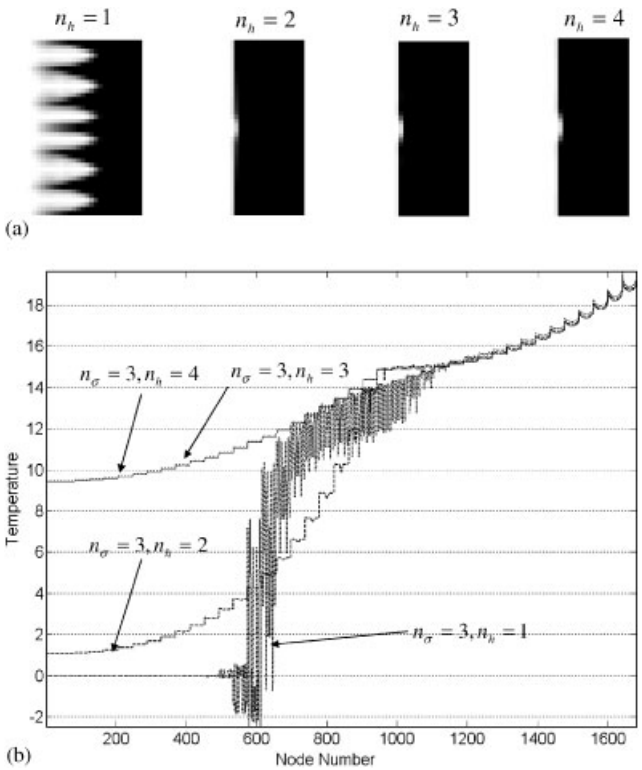

Figure 18. The optimized result for Problem A by the SIMP approach with varying values of n_h ($n_\sigma = 3$ fixed): (a) the density distribution; and (b) the temperature plot.

The result obtained by the present ECP is shown in Figure 19. The raster image shown in Figure 19(b) appears somewhat better in identifying the final optimal shape than the skeleton image in Figure 19(a), and the temperature distribution inside the whole design domain turned out to be feasible: see Figures 19(c) and (d).

The effect of the penalty exponent n_l on the optimized result in the ECP method is similar to its effect in the SIMP method. Since the link stiffness behaves as $l_0\gamma^{n_l}$, l_0 should be sufficiently large to simulate the rigid connection when $\gamma = 1$ but should not be too large in order to simulate no connection when $\gamma = \gamma_{\text{lower}}$ ($\gamma_{\text{lower}} = 0.01$). Thus, if l_0 becomes too large, the value of $l_0\gamma_{\text{lower}}^{n_l}$ increases and thus grey areas tend to appear, as seen in Figure 20. To reduce the intermediate design, we can use higher values for n_l. The effect of n_l on the optimized results is illustrated in Figure 21.

Figures 22 and 23 show the results obtained for Problem B by the element-density-based SIMP approach and by the ECP approach, respectively. The observations made for Problem A apply equally to the results obtained for Problem B.

Figures 24 and 25 show the results obtained for Problem C by the element-density-based SIMP approach and by the ECP approach, respectively. The observations made for Problem A apply equally to the results obtained for Problem C.

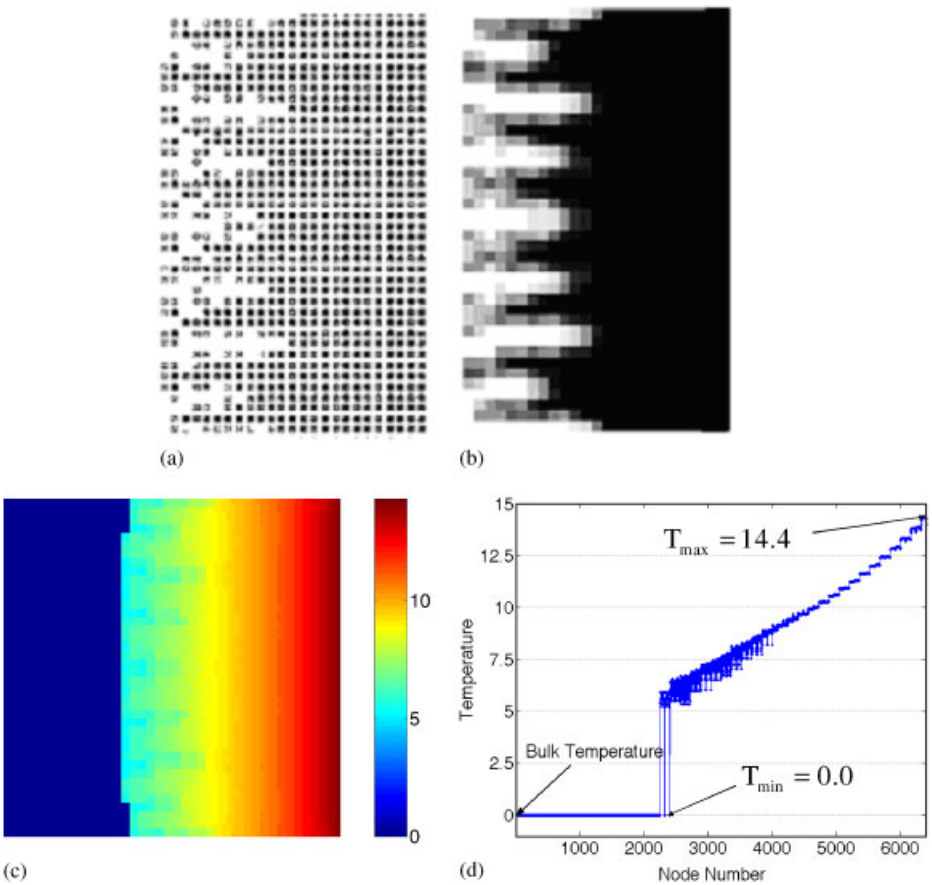

Figure 19. A result for Problem A by the ECP approach ($\gamma_{\text{lower}} = 0.01$, $l_0 = 1000$, $n_l = 3$): (a) skeleton representation; (b) raster image representation; (c) temperature contour plot; and (d) nodal temperature distribution.

For the considered problems, some nodal temperatures computed by the element-density-based method turned out to be higher than they should; otherwise the thermal balance cannot be satisfied.

Case 2: Electro-thermal-compliant actuator design.
The specific design problem definition is given in Figure 26. For elastic deformation analysis, the geometrical non-linearity (see Appendix A) was taken into account. To suppress the formation of checkerboard patterns, the sensitivity was averaged using the sensitivities at adjacent connections. For instance, the sensitivity $\partial u_s/\partial \gamma_p$ at Connection p is replaced by

$$\frac{\mathrm{d}\bar{u}_s}{\mathrm{d}\gamma_p} = \left(\frac{\mathrm{d}u_s}{\mathrm{d}\gamma_p} + \sum_{q=1}^{4} \frac{\mathrm{d}u_s}{\mathrm{d}\gamma_q} \right) \Big/ 5 \tag{29}$$

where q denotes the connection points near connection p.

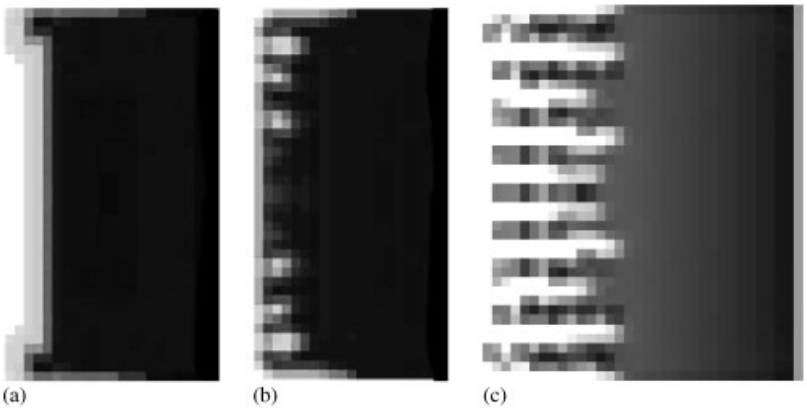

Figure 20. The effect of the link stiffness upper bound l_0 on the optimized solution ($n_l = 3$): (a) $l_0 = 10$; (b) $l_0 = 100$; and (c) $l_0 = 1000$.

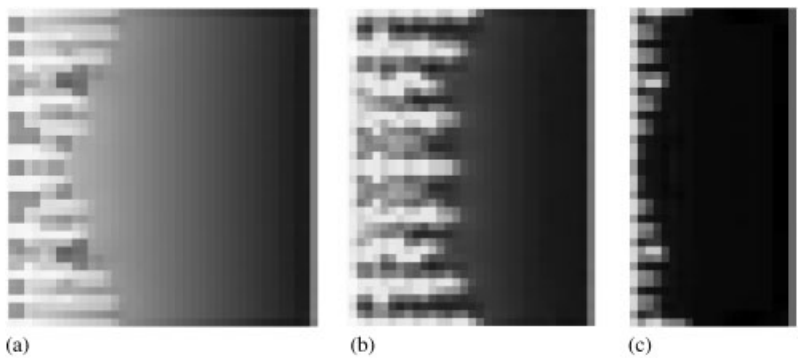

Figure 21. The effect of the link stiffness penalty exponent ($l_0 = 1000$ was used): (a) $n_l = 1$; (b) $n_l = 4$; and (c) $n_l = 8$.

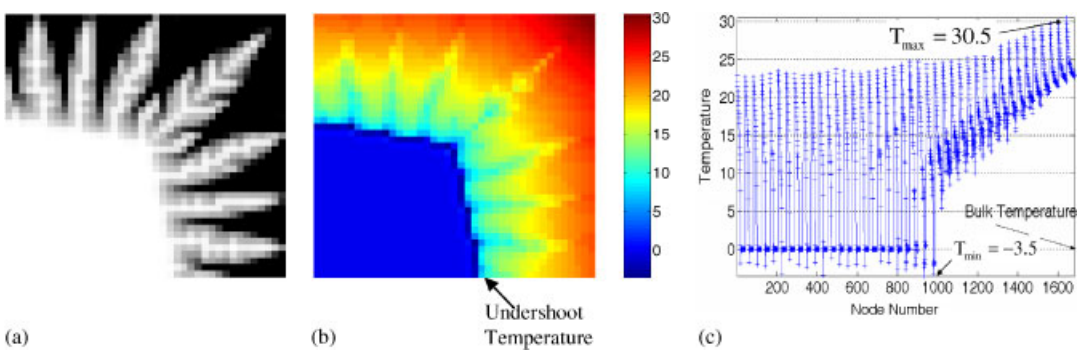

Figure 22. The optimized result for Problem B by the SIMP approach ($n_\sigma = 3$, $n_h = 0$): (a) density distribution; and (b) temperature inside the design domain.

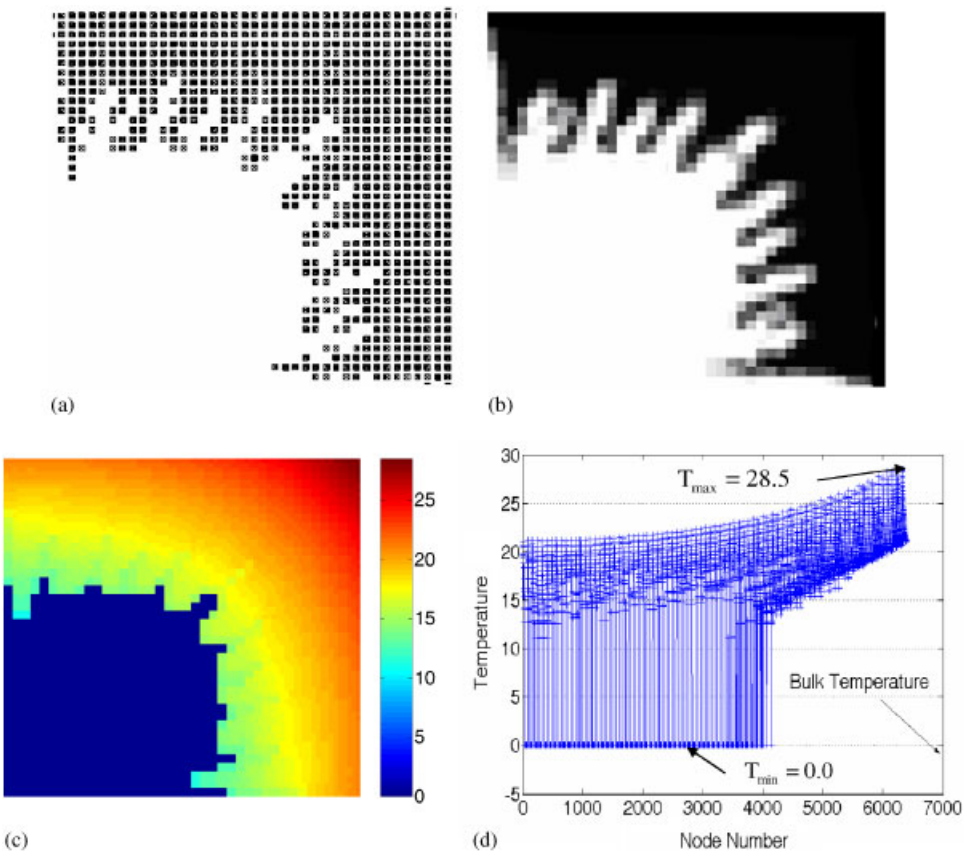

Figure 23. A result for Problem B by the ECP approach ($\gamma_{\text{lower}} = 0.01$, $l_0 = 1000$, $n_l = 3$): (a) skeleton representation; (b) raster image representation; (c) temperature contour plot; and (d) nodal temperature distribution.

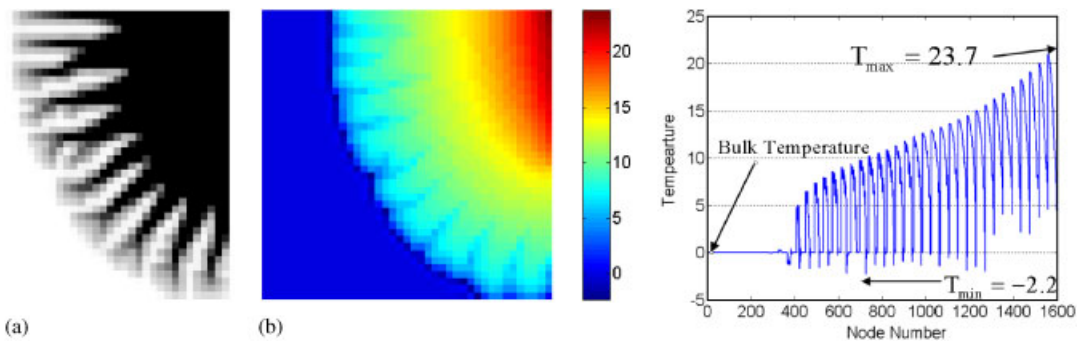

Figure 24. The optimized result for Problem C by the SIMP approach ($n_\sigma = 3$, $n_h = 0$). (a) density distribution; and (b) temperature inside the design domain.

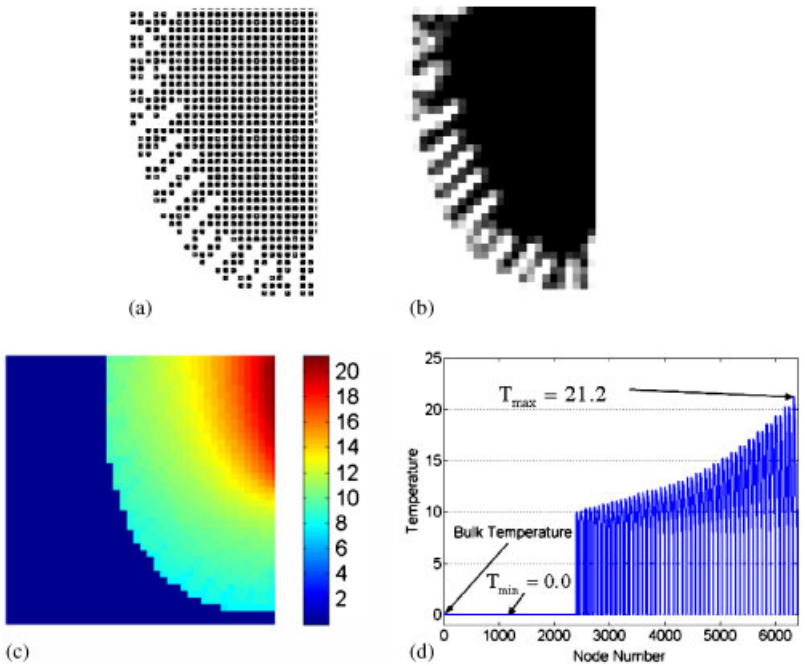

Figure 25. A result for Problem C by the ECP approach ($\gamma_{\text{lower}} = 0.01$, $l_0 = 1000$, $n_l = 3$): (a) skeleton representation; (b) raster image representation; (c) temperature contour plot; and (d) nodal temperature distribution.

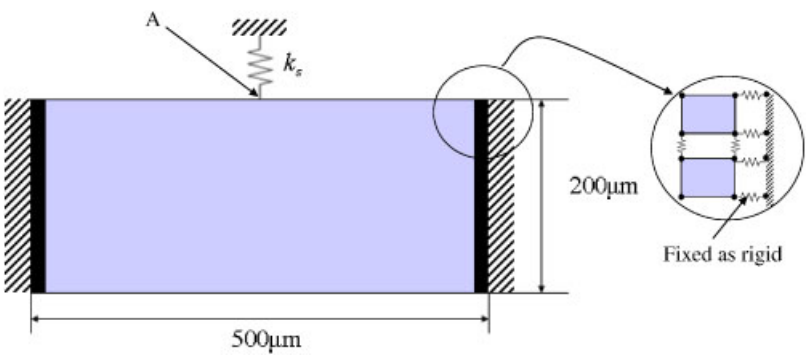

Figure 26. The problem definition for the design of an electro-thermal-compliant actuator. ($k_s = 100$ N/m, Young's modulus $= 200$ GPa, Poisson's ratio $= 0.31$, depth $= 15\,\mu$m, electric conductivity $= 6.4 \times 10^6$ K/Ω m, thermal conductivity $= 90.7$ W/K m, convection coefficient $= 18.7 \times 10^3$ W/m^2 K, thermal expansion coefficient $= 15 \times 10^{-6}$ K^{-1}, applied voltage $V_0 = 0.3$ V).

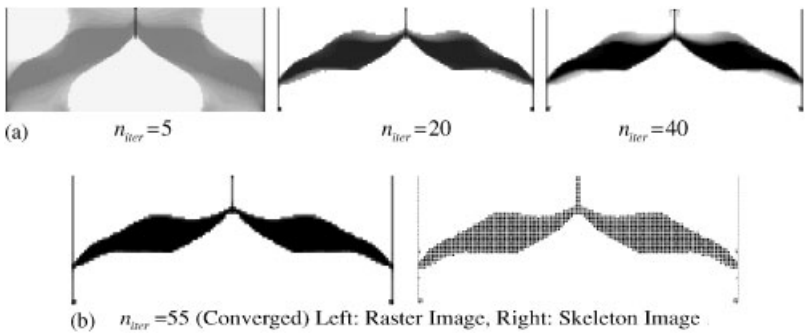

Figure 27. A result using the element connectivity method without the side convection model: (a) the intermediate results; and (b) the converged result (n_{iter}: the iteration number).

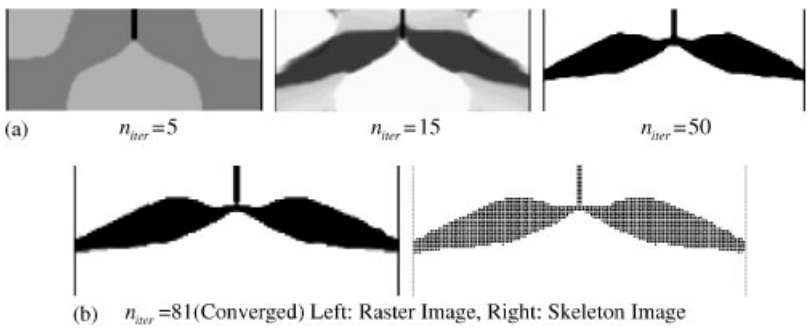

Figure 28. A result obtained by the element connectivity method with the side convection model: (a) intermediate results; and (b) the converged result (n_{iter}: the iteration number).

Figures 27 and 28 show the results by the ECP method without and with the consideration of the side convection. The mass constraint was 30%. When the side convection was considered, the interpolation scheme proposed in (27) was employed. The temperature distributions at the converged state are plotted in Figures 29(a) and (b). The effect of the consideration of the side convection on the optimal actuator layout was not significant, but the output displacement by the optimal actuator designed with the side convection was smaller than that without the side convection. This is because more heat is dissipated when the side convection is taken into account. When the input voltage becomes larger, the consideration of the side convection will become more important as shown in Figure 29(c). Note that the output displacements u_s in Figure 29 were calculated based on the geometrically non-linear deformation.

5. CONCLUSIONS

The topology optimization of multiphysics problems was newly formulated by the element connectivity parameterization method, with a special emphasis on heat transfer problems. First, it was shown that when more than one physical property needs to be interpolated as the

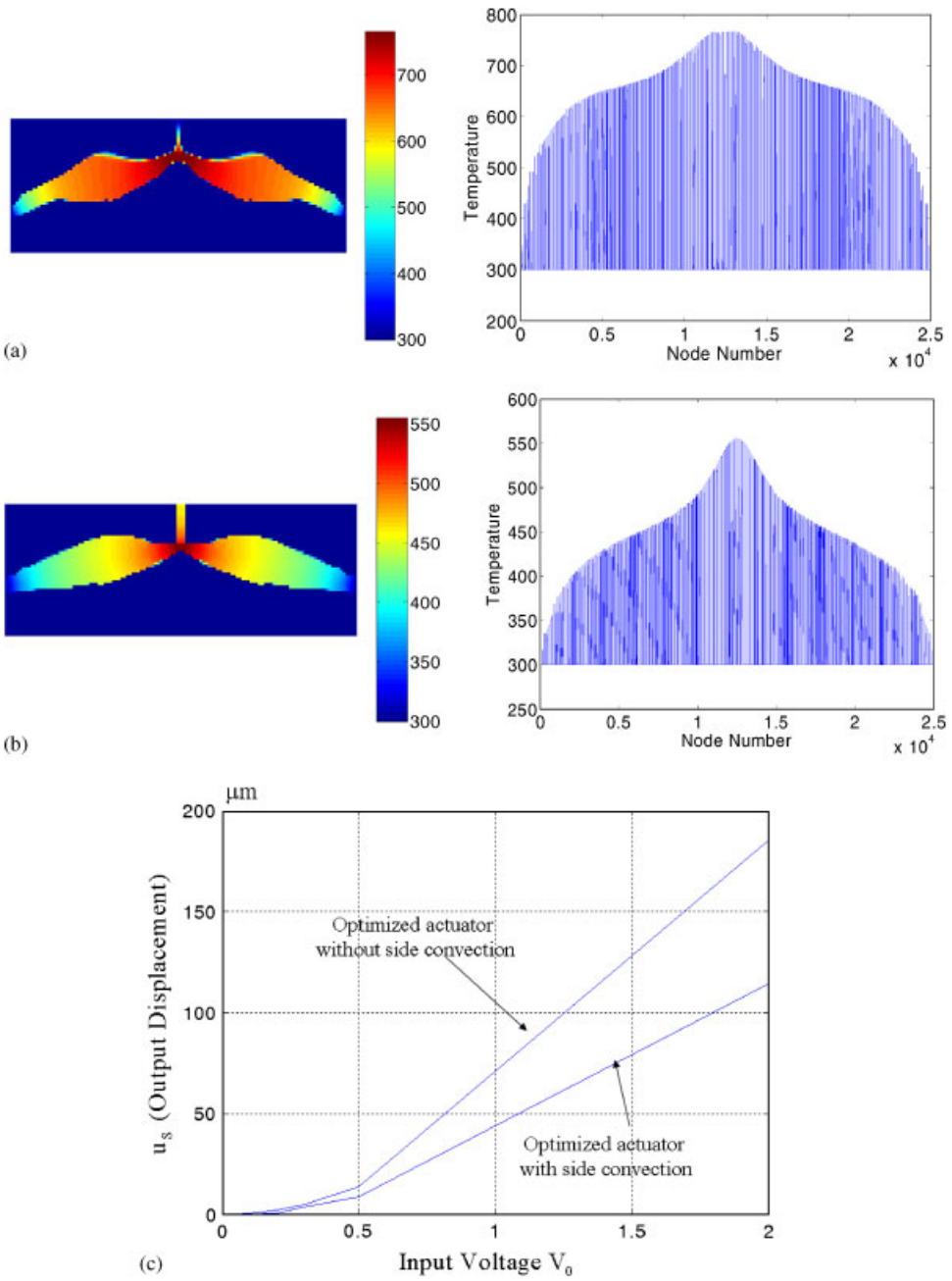

Figure 29. Temperature distribution of the optimized results: (a) temperature of a result without the side convection; (b) temperature of a result with the side convection; and (c) output displacements with the various input voltage.

functions of the element density variable in the standard element-density-based method, infeasible solutions can be obtained. Regardless of the interpolation functions employed, it is difficult or impossible to avoid infeasible solutions as long as the element densities are used as the design variables of topology optimization. Second, a new element connectivity parameterization formulation was developed to avoid infeasible solutions for multiphysics problems. The idea was to connect finite elements using sets of one-dimensional zero-length links, so a desired structural layout was represented by the element connectivity degree governed by the value of the link stiffness. When this approach was used for the analysis and optimization involving heat transfer, no problem such as undershooting or overshooting appeared. Finally, satisfactory results were obtained when the proposed method was applied to optimize a heat-dissipating structure and an electro-thermal-compliant actuator.

APPENDIX A: THE GOVERNING EQUATIONS FOR ETC ACTUATOR ANALYSIS

To analyse electric, heat transfer, and structural systems, three field variables are introduced: u_{E} denoting the electro potential, u_{T} denoting the temperature, and u_{S} denoting the displacement. The boundary condition is assumed to be given either as the Dirichlet condition on $\Gamma_{u_{(\circ)}}$ or the Neumann boundary condition on $\Gamma_{t_{(\circ)}}$ ($\circ = \mathrm{E}, \mathrm{T}, \mathrm{S}$).

When the electric field is assumed to be independent of the thermal field and the structural deformation, the governing equation for u_{E} is written as

$$(\sigma_{\mathrm{E}} u_{\mathrm{E},i})_{,i} = 0 \quad \text{in } \Omega \quad \text{with } u_{\mathrm{E}} = \bar{u}_{\mathrm{E}} \quad \text{on } \Gamma_{u_{\mathrm{E}}} \tag{A1}$$

The symbol σ_{E} denotes the electric conductivity. The barred quantity denotes the value prescribed on the boundary $\Gamma_{u_{(\circ)}}$. The comma denotes the differentiation.

For semi-coupled analysis, the temperature distribution inside the analysis domain Ω can be obtained from the following form of Poisson's equation:

$$\begin{gathered}(\sigma_{\mathrm{T}} u_{\mathrm{T},i})_{,i} = \sigma_{\mathrm{E}} u_{\mathrm{E},i}^2 \quad \text{in } \Omega \\ u_{\mathrm{T}} = \bar{u}_{\mathrm{T}} \quad \text{on } \Gamma_{u_{\mathrm{T}}} \quad \text{and} \quad n_i(\sigma_{\mathrm{T}} u_{\mathrm{T},i}) = \bar{t}_{\mathrm{T}} \quad \text{on } \Gamma_{t_{\mathrm{T}}}\end{gathered} \tag{A2}$$

where the source term $\sigma_{\mathrm{E}} u_{\mathrm{E},i}^2$ denotes the Joule heat generated by the electric field. The prescribed heat flux input $\bar{t}_{\mathrm{T}}$ implies the boundary convection, and n_i denotes the component of the normal vector.

If the temperature distribution u_{T} is obtained from Equation (A2), the structural displacement u_{S} is obtained from the following equations:

$$\begin{gathered}s_{ij,j} = 0 \quad \text{(in the absence of the body force)} \quad \text{in } \Omega \\ u_{\mathrm{S}(i)} = \bar{u}_{\mathrm{S}(i)} \quad \text{on } \Gamma_{u_{\mathrm{S}}} \quad \text{and} \quad s_{ij,j} n_j = \bar{t}_{\mathrm{S}(j)} \quad \text{on } \Gamma_{t_{\mathrm{S}}}\end{gathered} \tag{A3}$$

To take into account geometrical non-linear deformation, the second Piola–Kirchhoff stress tensor s_{ij} is used, which is related to the Green–Lagrangian strain η_{ij} as

$$s_{ij} = E_{ijkl}(\eta_{kl} - \alpha_{kl}(u_{\mathrm{T}} - u_{\mathrm{T}}^{\infty})) \tag{A4}$$

where E_{ijkl} and α_{kl} denote the elasticity tensor and the thermal expansion coefficient. For the problem considered in this work, $\alpha_{kl} = \alpha$ was assumed. The definition of η_{ij} is

$$\eta_{ij} = \tfrac{1}{2}[u_{S(i,j)} + u_{S(j,i)} + u_{S(k,i)}u_{S(k,j)}] \tag{A5}$$

The finite element formulation of Equations (A1)–(A3) may be found in most books on the finite element method. In this investigation, the notation in Reference [9] was used.

ACKNOWLEDGEMENTS

For this research, the first author was supported by the Korea Research Foundation Grant funded by Korea Government (MOEHRD, Basic Research Promotion Fund) (KRF-2004-214-M01-2004-000-20114-0).

REFERENCES

1. Bendsøe MP, Sigmund O. *Topology Optimization Theory*, *Methods and Applications*. Springer: New York, 2003.
2. Sigmund O. Design of multiphysics actuators using topology optimization—part I: one material structure. *Computer Methods in Applied Mechanics and Engineering* 2001; **190**(49–50):6577–6604.
3. Luzhong Y, Ananthasuresh GK. A novel topology design scheme for the multiphysics problems of electro-thermally actuated compliant micromechanisms. *Sensors and Actuators A* 2002; **97–98**:599–609.
4. Yoon GH. Geometrical nonlinear topology optimization with feature scale control. *School of Mechanical and Aerospace Engineering*. Seoul National University: Seoul, Korea, 2004.
5. Yoon GH, Kim YY. Element connectivity parameterization for topology optimization of geometrically nonlinear structures. *International Journal of Solids and Structures* 2005; **42**(7):1983–2009.
6. Bruns TE, Tortorelli DA. An element removal and reintroduction strategy for the topology optimization of structures and compliant mechanisms. *International Journal for Numerical Methods in Engineering* 2003; **57**:1413–1430.
7. Buhl T, Petersen CBW, Sigmund O. Stiffness design of geometrically nonlinear structures using topology optimization. *Structural and Multidisciplinary Optimization* 2000; **19**(2):93–104.
8. Cho SH, Jung HS. Design sensitivity analysis and topology optimization of displacement-loaded nonlinear structures. *Computer Methods in Applied Mechanics and Engineering* 2003; **192**:2539–2553.
9. Bathe KJ. *Finite Element Procedures*. Prentice-Hall: Englewood Cliffs, NJ, 1996.
10. Daryl LL. *A First Course in the Finite Element Method*. PWS Publishing Company: Boston, 1993.
11. Svanberg K. The method of moving asymptotes—a new method for structural optimization. *International Journal for Numerical Methods in Engineering* 1987; **24**:359–373.
12. Zillober C. SCPIP—an efficient software tool for the solution of structural optimization problems. *Structural Multidisciplinary Optimization* 2002; **24**:362–371.

